T.R.
BOLU ABANT İZZET BAYSAL UNIVERSITY
INSTITUTE OF GRADUATE STUDIES
Department of Physics

ASSESSMENT OF MECHANICAL DEFORMATION PROCESSES THROUGH MICRO-HARDNESS TESTS OF SUPERCONDUCTING MGB2 WIRE SAMPLES MADE WITH STANDARD AND POWDER INTERNAL MAGNESIUM DIFFUSION TECHNIQUES

MASTER OF SCIENCE

MUEEZ UR REHMAN

ACADEMIC SUPERVISOR
Prof. Dr. İbrahim BELENLİ

BOLU, JULY - 2023

APPROVAL OF THE THESIS

Assessment of Mechanical Deformation Processes through Micro-Hardness Tests of Superconducting MgB_2 Wire Samples Made with Standard and Powder Internal Magnesium Diffusion Techniques submitted by **Mueez Ur REHMAN** and defended before the Examining Committe Members listed below in partial fulfillment of the requirements for the degree of **Master of Science** in **Department of Physics, Institute of Graduate Studies of Bolu Abant Izzet Baysal University in 28.07.2023** by

Examining Committee Members	**Signature**
Supervisor Prof. Dr. İbrahim BELENLİ Bolu Abant Izzet Baysal University	....
Member Prof. Dr. Hakan YETIŞ Bolu Abant Izzet Baysal University	....
Member Prof. Dr. Ali GENCER Ankara University	....

Prof. Dr. İbrahim KÜRTÜL

Director of Instıtute of Graduate Studies

ETHICAL DECLARATION

In this thesis dissertation that was properly prepared according to the Thesis Writing Rules of Bolu Abant İzzet Baysal University of the Institute of Graduates Studies, I hereby declare that;

- All data, information, and documents presented in the thesis were obtained in accordance with the academic and ethical rules,
- All data, documents, assessments, and results were presented in accordance with the scientific ethical and moral rules,
- All works that were benefitted in the thesis were appropriately cited,
- No alteration was made in the data used,
- Study presented in this thesis is original,

Otherwise, I declare that I accept the loss of all my rights in case any contradiction that may arise against me.

Based on the plagiarism report that was generated on the date of 22/06/2023 by using predetermined filtrations set by Directorate of Institute of Graduate Studies of the Turnitin programme, a plagiarism detection sofware, the similarity index detected was 29%.

Mueez Ur REHMAN

ABSTRACT

ASSESSMENT OF MECHANICAL DEFORMATION PROCESSES THROUGH MICRO-HARDNESS TESTS OF SUPERCONDUCTING MGB2 WIRE SAMPLES MADE WITH STANDARD AND POWDER INTERNAL MAGNESIUM DIFFUSION TECHNIQUES
MSC THESIS
MUEEZ UR REHMAN
BOLU ABANT IZZET BAYSAL UNIVERSITY
INSTITUTE OF GRADUATE STUDIES
DEPARTMENT OF PHYSİCS
(SUPERVISOR: PROF. DR. İBRAHİM BELENLİ)

BOLU, JULY 2023
(xiii + 55)

This research aims to investigate the mechanism of superconductivity and the production of MgB_2 wires. The generation of high magnetic fields in practical applications requires long, homogeneous superconducting MgB_2 wires. Various techniques, including the powder-in-tube (PIT) method and internal magnesium diffusion (IMD) technique, are employed to obtain superconducting wires. This study specifically focuses on the PIT method and IMD technique to create the MgB_2 phase. The effect of hardness will be examined using HV tests, as the hardness of the constituents of the composite MgB_2 wire is modified during the cold drawing process. The cross sections of the wire samples will be analyzed to determine if the regions of boron, magnesium and iron exhibit different HV results between the Standard and Powder IMD methods. This research aims to relate these findings with the mechanical behavior, superconducting properties, structure and microstructure of MgB_2, whether the microhardness values do or do not differ.

KEYWORDS: MgB_2, IMD, HV, Superconducting Wire, Mg Diffusion

ÖZET

STANDART VE TOZ DAHİLİ MAGNEZYUM DİFÜZYON TEKNİKLERİYLE YAPILAN SÜPERİLETKEN MGB2 TEL NUMUNELERİN MEKANİK DEFORMASYON SÜREÇLERİNİN MİKRO-SERTLİK TESTLERİ İLE DEĞERLENDİRİLMESİ
YÜKSEK LİSANS TEZİ
Mueez Ur REHMAN
BOLU ABANT İZZET BAYSAL ÜNİVERSİTESİ
LİSANSÜSTÜ EĞİTİM ENSTİTÜSÜ
FIZIK ANABİLİM DALI

(TEZ DANIŞMANI: PROF. DR. İBRAHİM BELENLİ)

BOLU, TEMMUZ - 2023
(xiii + 55)

Bu araştırma, süperiletkenlik mekanizmasını ve MgB_2 tellerinin üretimini araştırmayı amaçlamaktadır. Pratik uygulamalarda yüksek manyetik alanların oluşturulması, uzun, homojen süperiletken MgB_2 telleri gerektirir. Süperiletken teller elde etmek için tüp içinde toz (PIT) yöntemi ve dahili magnezyum difüzyon (IMD) tekniği dahil olmak üzere çeşitli teknikler kullanılır. Bu çalışma özellikle MgB_2 fazını oluşturmak için PIT yöntemi ve IMD tekniğine odaklanmaktadır. Kompozit MgB_2 telinin bileşenlerinin sertliği soğuk çekme işlemi sırasında değiştirildiğinden, sertliğin etkisi HV testleri kullanılarak incelenecektir. Bor, magnezyum ve demir bölgelerinin Standart ve Toz IMD yöntemleri arasında farklı HV sonuçları gösterip göstermediğini belirlemek için tel numunelerinin enine kesitleri analiz edilecektir. Bu araştırma, mikrosertlik değerleri farklı olsun veya olmasın, bu bulguları MgB_2'nin mekanik davranışı, süperiletken özellikleri, yapısı ve mikro yapısı ile ilişkilendirmeyi amaçlamaktadır.

ANAHTAR KELİMELER: MgB_2, IMD, HV, Süperiletken Tel, Mg Difüzyonu

TABLE OF CONTENTS

LIST OF FIGURES

Page

LIST OF TABLES

Page

LIST OF ABBREVIATIONS AND SYMBOLS

LTS	: Low Temperature Superconductors
HTS	: High Temperature Superconductors
BEC	: Bose Einstein Condensation
BCS	: Bardeen-Cooper-Schrieffer
PIT	: Powder In Tube
IMD	: Internal Magnesium Diffusion
CTFF	: Continous Tube Filling and Forming
HIP	: High Isostatic Pressure
ZFC	: Zero Field Cooling
SQUID	: Superconducting Quantum Interference Device
HCP	: Hexagonal Close Pack
AIMI	: Advanced Internal Magnesium Infiltration
HV	: Vickers Hardness
DC	: Direct Current
J	: Current Density
J_c	: Critical Current Density
J_{ce}	: Engineering Critical Current Density
T_c	: Critical Temperature
α	: Isotope Effect Coefficient
ξ_0	: Coherence Length
V	: Voltage
ρ	: Resistivity

ACKNOWLEDGEMENTS

I would like to convey my utmost appreciation and gratitude to my esteemed supervisor, Prof. Dr. Ibrahim Belenli, for his exceptional dedication, guidance, kindness and invaluable professional advice throughout the completion of this study. I am sincerely grateful for his insightful remarks and valuable suggestions.

Also, I would like to express my profound gratitude to Prof. Dr. Hakan Yetiş for his unwavering guidance and expertise on superconductivity, which immensely aided my comprehension during my research journey. Additionally, I owe a heartfelt thank to my colleague Doğan Avcı for his kindness, and his contribution to the preparation of this study.

I want to express my sincere gratitude to the committee members, the Institute of Graduate Studies, and the faculty members of the Physics Department at Bolu Abant Izzet Baysal University, where I successfully completed my postgraduate studies.

I am deeply grateful to my friends, especially Dr. Omer Can Unuvar, who have provided unwavering support and motivation throughout this journey. I feel incredibly fortunate to have all of you in my life, and I want to express my heartfelt appreciation for your assistance. Thank you from the depths of my heart.

Lastly, I would like to extend my heartfelt thanks to my entire family, with a special mention of my parents, for their unwavering support and constant encouragement. This study would not have been possible without your unconditional dedication.

1. INTRODUCTION

The great Dutch physicist Heike Kamerlingh Onnes, on 10th of July 1908, experienced the wonderful moment of his career. That was the day when he liquefied Helium (He), measured the resistance of mercury at very low temperature as shown in Figure 1.1 and started a new chapter of Low Temperature Physics (1). Superconducting behaviour was discovered more than a century ago and it took long time to understand its physics. As its name suggests, a conductor after becoming superconducting, does not show any resistance for the electrical conduction. Mostly materials show this behaviour at very low temperatures.

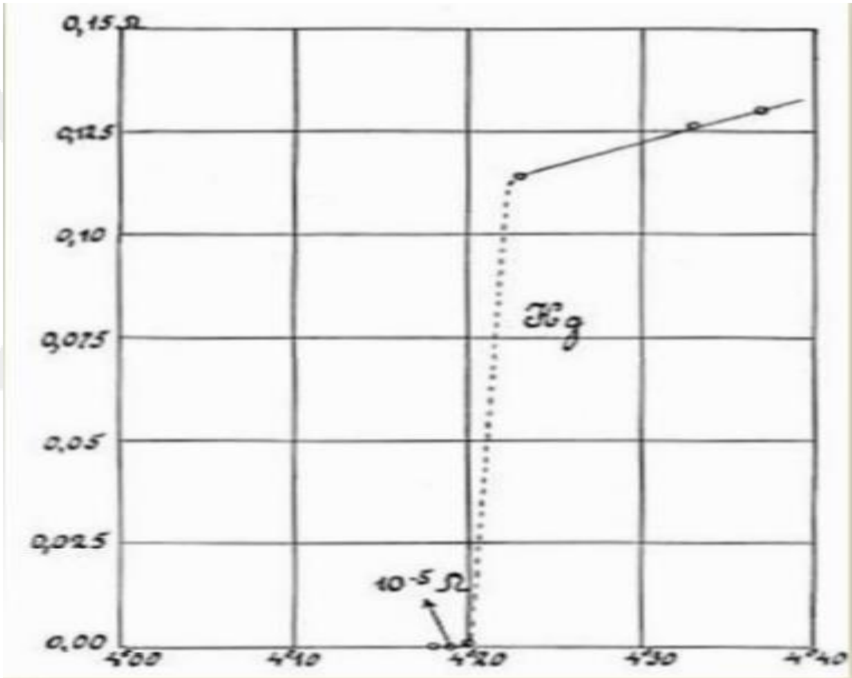

Figure 1.1. Resistance and temperature relation of mercury (2).

1.1 Historical Background

Before Kamerlingh Onnes, electrical conduction was understood and it was established that the charge transport is influenced by electrons. Additionally the resistance of many metals had been measured and it was discovered that near room temperature, resistance decreases linearly with decreasing temperature. There were three possibilities to be discussed regarding resistance at very low temperatures (1).

1. As the temperature drops, the resistance might become zero (Figure 1.2, curve 1).

2. There is a possibility for it to reach a finite limit (Figure 1.2, curve 2).
3. At very low temperatures, it could go through a minimum and get close to infinity as the temperature approaches to zero Kelvin (Figure 1.2, curve 3)

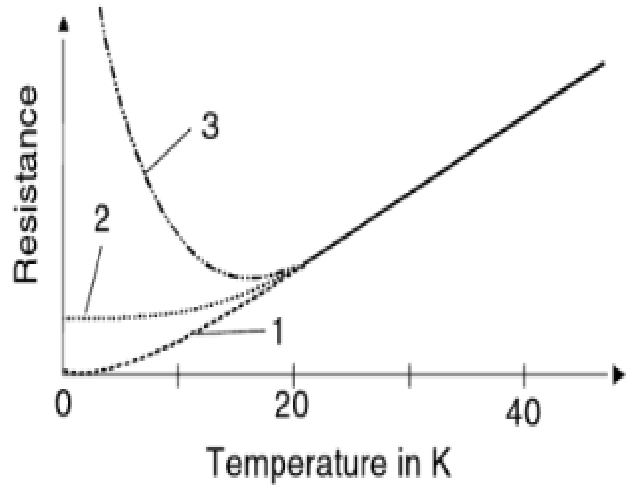

Figure 1.2. Illustration of temperature dependent electrical resistance (1).

The great Dutch physicist Heike Kamerlingh Onnes, in 1911, discovered the phenomenon of superconductivity on mercury when he cooled it to liquid helium temperature (2). He received Nobel Prize in 1913 for this incredible discovery. Since then, this discovery raised new hopes of completely changing the world of technology. This event arises the possibility of making superconducting wires that will carry current from stations to homes with zero voltage, namely the power loss $P = I^2R$ consumed is zero, this will make power consumption and distribution very cheap. It had the possibility to completely change the world and that is why the discovery of superconductivity considered very important and until date it is still considered as an important area. After this remarkable discovery of superconductivity, researchers got interested in studying the behaviour of materials at very low temperatures.

In 1933, W. Meissner and R. Ochsenfeld (3) German researchers discovered that superconductors could levitate a magnet in superconducting state, repulsion of magnetic field, which known as Meissner effect. In 1950, a similar experiment “isotope effect” was conducted by two different laboratories, Renolds et al (4) at Rutgers university and at National Bureau of Standards (5). This experiment showed that there is inversely relation between critical temperature T_c and square root of average isotopic mass of material. After these discoveries, scientists were curious to understand the physics of superconductivity and the absence of resistance below T_c.

Two basic phenomena in superconductors, zero resistance and the Meissner effect, could not be explained using classical theory. In 1935, Superconductivity as a macroscopic quantum effect defined by (the London brothers) F. London and H. London (6) by deriving electrodynamics equations. Their theory is established on two equations. The first equation (2.1) shows that the change in superconducting current density J_s with time is proportional to the electric field **E** and second equation explains the relationship between superconducting current density and magnetic field **B**. So, the London equations successfully explain the zero resistance, Meissner effect and estimate the existence of penetration depth in superconductor (6).

$$\frac{\partial j_s}{\partial t} = \frac{n_s e^2}{m}\boldsymbol{E} \qquad \mathbf{(2.1)}$$

$$\nabla \times j_s = \frac{n_s e^2}{m}\boldsymbol{B} \qquad \mathbf{(2.2)}$$

In 1953, an additional parameter, coherence length ξ_0, was added to London’s equations by Pippard (7). He postulated that when superconducting electrons are in close proximity, they exhibit correlations, and this distance limit was termed the coherence length ξ_0. Additionally, Pippard made an estimation of the mean-free-path l for superconducting electrons and compared it with the coherence length ξ_0 to determine the behavior of the superconductor in both the ‘clean’ ($l >> \xi_0$) and ‘dirty’ ($l << \xi_0$) limit (7).

Pippard’s theory was incomplete and published in 1953. An argument was proposed by J.Bardeen (8) that an energy gap would be required if a coherence is present in superconducting state. Superconducting materials exhibit an energy gap between their normal and superconducting states. The relation between density of states and energy of metal at normal and superconducting states is shown in Figure 1.3.

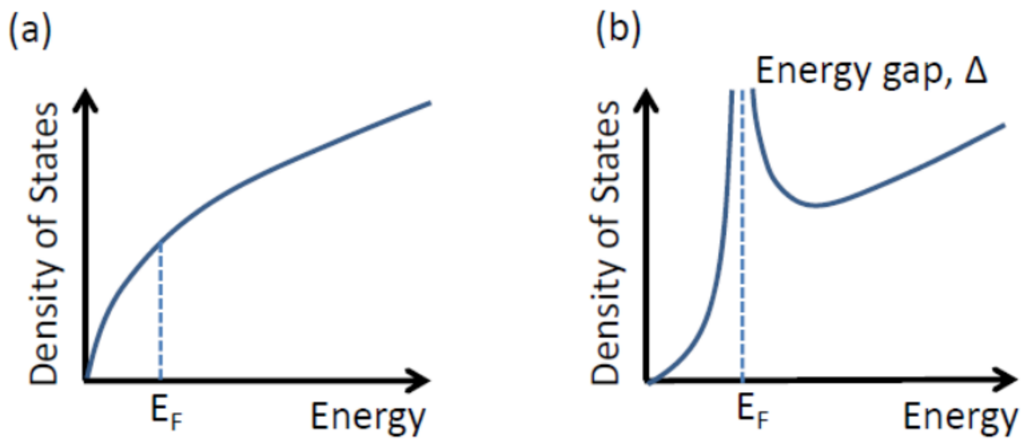

Figure 1.3. Density of states versus energy for conductor in (a) normal state and in (b) superconducting state (9).

Afterwards, L. Cooper (10) successfully estimated that such an energy gap can be perceived by having a bound state between two electrons in superconducting state. In 1957, Bardeen and Cooper collaborated with R. Schrieffer (11) to propose a theory that would contain the current predictions of superconductivity and soon introduced the BCS theory of superconductivity.

In the BCS theory, superconductivity is mediated by and dependent on phonons. Two electrons attract each other via an interaction between the vibrations of lattice and each of the two electrons. These two electrons form a so-called ‘Cooper pair’ as shown in Figure 1.4. Electrons of cooper pairs have opposite spins to each other, and total momentum is zero. As a result, they can condense at ground state via Bose-Einstein Condensation (BEC). Once this phenomenon takes place, superconducting electrons are in the form of cooper pairs, then it requires energy to break a single pair and produce two electrons. So, that specific energy which is required to break a single pair is defined as energy gap (2Δ). The density of states, superconducting electrons (cooper pairs) will remain in superconducting state until enough energy is given to system equivalent or higher than energy gap to break cooper pairs.

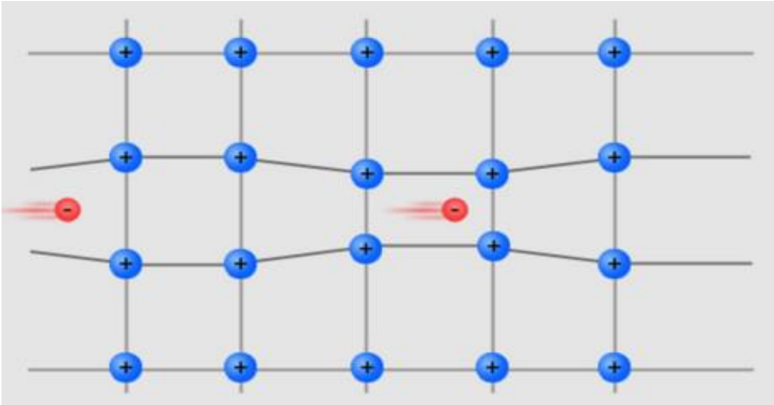

Figure 1.4. Attraction between two electrons caused by lattice vibration (12).

In 1962, another major achievement occurred when Brian D. Josephson (13), a graduate student at Cambridge University, proposed the idea that an electrical current can flow between two superconductors that are separated by a non-superconducting material or insulator. Later on, this prediction was confirmed by an experiment, in which there was tunnelling of electrical current between superconductors. This tunnelling phenomenon named as Josephson Effect. By using this idea, new electronic devices have been built as SQUIDS which are capable to detect very weak magnetic fields.

The period of 1986 was revolutionary step for the field of superconductivity, when Alex Muller and Georg Bednorz (14), two researchers at the IBM Research Laboratory in Switzerland prepared a ceramic which showed the behaviour of superconductivity at 30 K, which was highest temperature that time. They received Nobel Prize in 1987 for the discovery of superconducting copper oxides (cuprates). The discovery of superconductivity in ceramics was so surprising because ceramics are electrical insulators or very bad conductors at room temperature. The behaviour of superconductivity in ceramics is very interesting and has not been understood completely. The ceramic was synthesized of Lanthanum (La), Barium (Ba), Copper (Cu) and Oxygen (O) elements. A research team at University of Alabama-Huntsville (15) performed an experiment, in January of 1987, in which they substituted Yttrium for Lanthanum in the compound discovered by Muller and Bednorz. This substitution causes the rise in T_c from 30 K to 92 K in YBCO. Afterward, a high T_c ceramic superconductor in mercuric-cuprates was synthesized with transition temperature of 134 K, by the team of Schilling et al (16) of Zurich, Switzerland.

In 2001, Nagamatsu et al. (17) discovered superconductivity in MgB_2, a simple binary compound of magnesium Mg and boron B, having a remarkable T_c of 39 K. Due to its high critical temperature among conventional superconductors and easy fabrication in the form of long wires and tapes, MgB_2 superconductors have a good chance to replace conventional superconductors NbTi and Nb_3Sn in high magnetic field applications (18).

1.2 Fundamentals of Superconductivity

The state of a superconductor is determined by three critical parameters, namely the critical temperature T_c, critical current density J_c and critical magnetic field H_c. The relationship among these parameters is shown in Figure 1.5. To sustain superconducting state, all of these parameters should remain below the critical values.

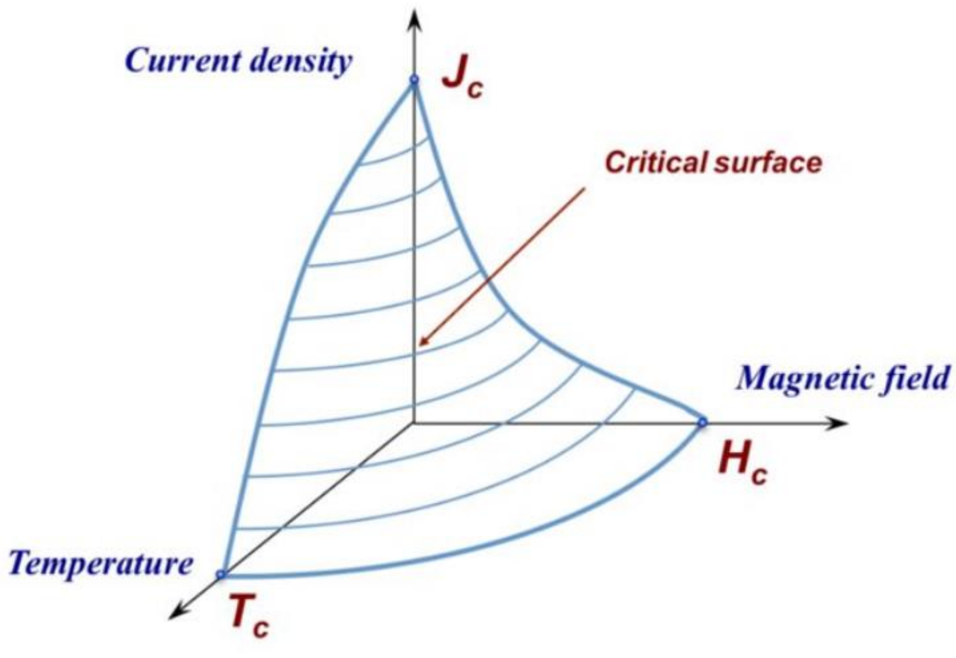

Figure 1.5. Critical surface as superconducting region below these parameters (19).

1.3 The Cooper Pairs

Whenever a superconducting material is cooled below its T_c, it changes from normal state to superconducting state. In the superconducting state, superconducting electrons flow in pairs which is called cooper pair and this pairing is influenced by interaction between the electrons and phonons in the material (11).

Two electrons with opposite momentum and spin form a pair with a net momentum of zero. In MgB_2, the two types of atoms, magnesium Mg and boron B, form layers in the crystal structure. The superconductivity in MgB_2 is mainly attributed to the B atoms, which form a hexagonal network of covalent bonds that provide a channel for the formation of Cooper pairs (20).

1.4 Coherence Length

It is a measure of distance over which superconductivity is maintained. It is defined as the characteristic length scale over which the wave function of Cooper pairs, which are responsible for superconductivity in the material, remains coherent (11). The coherence length, which is a fundamental length scale, varies as a function of temperature.

$$\xi_0^2(T) = \frac{\hbar^2}{2m^* a(T)} \tag{2.3}$$

Where 2m* is the mass of a superconducting electrons in a cooper pair and a(T) is a temperature dependent parameter in the Ginzburg-Landau (GL) equation:

$$a(T) \approx a_0[(T/T_c) - 1] \tag{2.4}$$

1.5 The Penetration Depth

The remarkable feature of superconductor is that exclusion of external magnetic field by forming surface shielding currents. So, whenever a superconductor is placed in an external magnetic field, the magnetic field penetrates the material from the surface for a specific distance, this specific distance is called penetration depth (1). The depth of the surface layer where the shielding current enters is designated as the penetration depth λ, and it varies with temperature according to the equation (2.5).

$$\lambda(T) = \frac{\lambda_0}{\sqrt{1 - (T/T_c)^4}} \tag{2.5}$$

In above equation, λ_0 represents the penetration depth at 0K and it is a characteristic of a material.

1.6 The Meissner Effect

The characteristic of a superconductor that differs it from a perfect conductor is the Meissner effect. In 1933, Robert Ochsenfeld and Walther Meissner (3) discovered that whenever a superconductor is placed in a magnetic field, it does not allow the existence of magnetic flux density in the interior of superconducting material. So, the magnetic field inside a type- I superconductor is zero. This effect arises due to the perfect diamagnetism of the superconducting material, and is a consequence of the fact that in a superconductor, some of the free electrons form Cooper pairs and move without resistance. This phenomenon happens because the screening currents, induced on the surface of the superconductor or by the applied magnetic field, generate an interior field. These induced surface currents flow exactly in a direction to cancel the applied magnetic field within the material. But a perfect conductor (conductor with zero resistivity) does not show this phenomenon in normal state.

Figure 2.6 shows the presence of Meissner effect. For the demonstration of the Meissner effect in a laboratory, a magnetic field is applied to a superconductor sample either before or after cooling. These two situations are respectively called field cooling (FC) and zero field cooling (ZFC). A perfect conductor has zero resistivity and when a material with zero resistivity is subject to magnetic flux density changes, an emf is produced in accordance with Faraday's law of induction. This results in flow of the surface currents, which cancel the applied magnetic field inside the material.

In field cooling, if the superconductor is not below its critical temperature, then the applied magnetic field will keep penetrating it. After cooling below its T_c, the screening currents will flow on the surface of superconductor generating an opposing magnetic field and consequently, a repulsive force is generated to cancel the field in the interior of a superconductor. But in the case of perfect conductor as shown in Figure 1.6, it becomes perfect conductor when temperature is below its T_c and cooling it below its T_c in the presence of magnetic field does not make it to repel external magnetic field. So, in field cooling, perfect conductor and superconductor behave differently but in, zero field cooling, both behave in a same way.

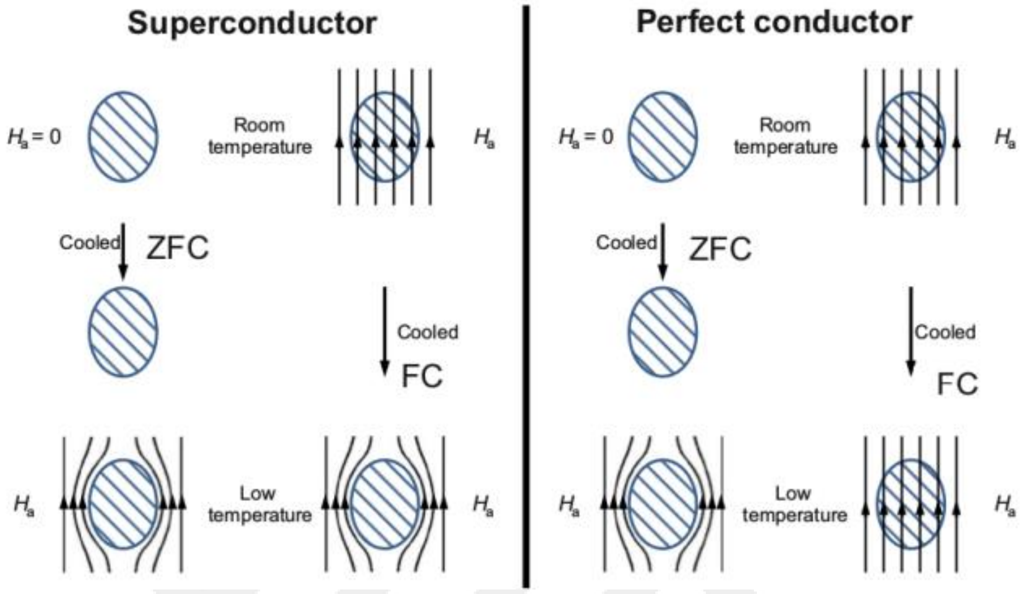

Figure 1.6. Illustration of magnetic behaviour for superconductor and perfect conductor (21).

1.7 Type-I and Type-II Superconductors

There are two groups of superconductors according to their behaviour in the presence of an applied magnetic field as shown in Figure 1.7. Type-I superconductors are characterized by a single critical magnetic field, above which the superconducting state is destroyed and the material becomes normal (non-superconducting). In type-I superconductors, the state of superconductivity is abruptly terminated when the magnitude of the applied magnetic field exceeds a critical value H_c. The sample's geometry can lead to an intermediate state with a baroque pattern which include regions of normal material carrying a magnetic field mixed with regions of superconducting material without a field. Examples of type-I superconductors include pure elements like mercury and lead etc.

Type-II superconductors have two critical magnetic fields, known as the lower H_{c1} and upper H_{c2} critical fields. When the external magnetic field applied to a Type-II superconductor is below the lower critical field H_{c1}, the applied field can be fully expelled and the material behaves similarly to a Type-I superconductor. However, when the field is increased above H_{c1} but below the upper critical field

H_{c2}, the magnetic flux cannot be completely excluded, and instead, it penetrates the superconductor partially in the form of vortices. This phenomenon is referred to as the mixed state. In a type-II superconductor, the vortices can move through the material if the material is in the mixed state, leading to dissipation of energy and a gradual transition to the normal state as the magnetic field is increased. Examples of type-II superconductors including high-temperature superconductors like MgB_2, $YBa_2Cu_3O_7$ and low temperature superconductors NbTi, Nb_3Sn etc.

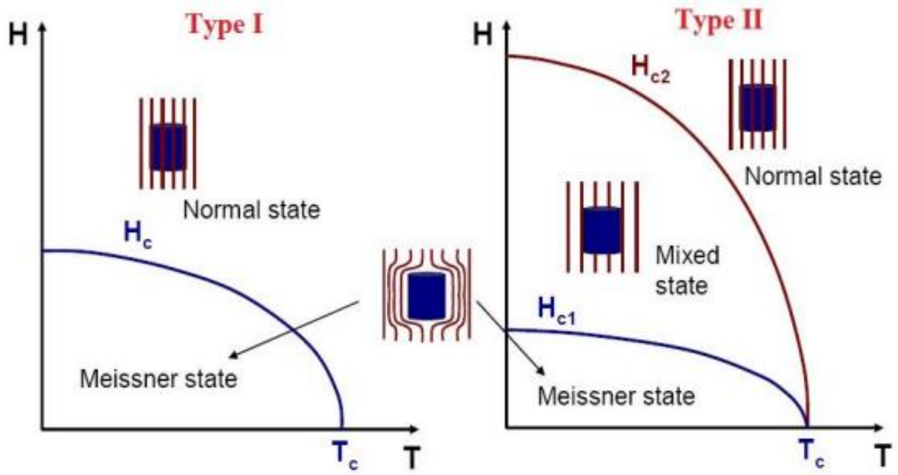

Figure 1.7. Phase diagram of Type I and Type II superconductors (22).

1.8 Practical Implications of Superconductors

The most useful superconductors are those that have the highest transition temperature and the highest critical current density under highest magnetic field. Currently, low-temperature superconductors (LTS), such as Nb_3Sn (T_c of 18K) and NbTi (T_c of 9K), are employed in various applications, including nuclear magnetic resonance (NMR), magnetic resonance imaging (MRI) and magnets for plasma fusion devices (18).

Nonetheless, the utilization of Nb_3Sn in low-field electromagnet applications can be costly due to the material's fragile nature, challenging manufacturing process and operation at liquid helium temperature. In contrast, high-temperature superconductors (HTS), such as bismuth strontium calcium copper oxide (BSCCO), specifically Bi-2223 (T_c of 110K), Bi-2212 (T_c of 85K) and $YBa_2Cu_3O_{7-x}$ (YBCO, T_c of 92K) are being employed in various electric power applications (15). The high cost of HTS and their unfavourable properties, such as high anisotropy, weak links and AC loss can result in undesirable factors during magnet fabrication (23).

Another class of superconductors that has been gaining attention are the iron-based superconductors, such as FeSe, LiFeAs, Fe(Se,Te), they have relatively high transition temperature (T_c of 20-30K). The challenge is the material’s quality, it's hard to get a large enough high quality single crystals.

Superconductors have a wide range of applications, including:

1. Magnetic Resonance Imaging (MRI) machines, which use superconducting magnets to create detailed images of the inside of the body.
2. High-energy particle accelerators, such as the Large Hadron Collider, which use superconducting magnets to accelerate particles to high speeds.
3. Power transmission and distribution, where superconductors can be used to transmit large amounts of electricity with minimal energy expenditure.
4. Electric power generation, such as wind and solar power, superconductors are used to increase the efficiency of the generators.
5. Sensors and detectors, for example, superconducting sensors are used in the search for dark matter and in the detection of gravitational waves.
6. High-speed trains, Maglev trains, which use superconducting magnets to levitate and propel the train, are being developed for high-speed transportation.
7. Superconductors have been used to create qubits, which are the basic building blocks of a quantum computer. Superconducting qubits are currently one of the most promising candidates for building large-scale quantum computers.

2. AIM AND SCOPE OF STUDY

The discovery of superconductivity in MgB_2, a binary intermetallic, by Jun Akimitsu in Japan was a remarkable leap among scientific community in applied superconductivity research. Immense research have been done to make it viable for commercial applications since then. Due to its remarkable properties as high critical temperature of 39K, simple crystalline structure, weak link free grain boundaries and low material cost make it potential candidate for replacing conventional Low Temperature Superconductors (LTS) and High Temperature Superconductors (HTS). Furthermore, MgB_2 has large coherence length and low anisotropy than HTS which make it more viable superconductor economically and technologically.

For the generation of high magnetic field, it requires homogenous and long MgB_2 wires. The performance of MgB_2 wires can be increased mainly by enhancing the critical current density J_c, which is the upper limit of capacity of carrying resistanceless current. Several approaches have been executed to enhance the J_c in MgB_2 wires, such as increasing grain connectivity, reducing porosity (voids), reduction of MgO content in ceramic core, addition of dopants and modifying the flux pinning mechanism. PIT is most common method for fabrication of long MgB_2 wires but wires fabricated by IMD method show higher J_c than the wires fabricated by PIT method.

In this work, standard and powder IMD wires were fabricated. Mechanical behaviour and homogeneity of structure are important for fabrication of long wires. The microhardness of iron, boron and magnesium regions of cold-drawn wires can be measured by Vickers Hardness tests. The results of these mechanical tests can be related to the superconducting performance of standard and powder IMD wires. Usually mechanical deformation causes hardening of material, but magnesium rod shows work softening behaviour and microhardness of magnesium powder increases more than that of pure magnesium rod during cold drawing. So, the aim of research is to evaluate mechanical and superconducting behaviour of powder and standard IMD wires, which will be helpful in future for the fabrication of long wires having the capacity to carry large amount of resistanceless currents to generate magnetic fields.

3. MAGNESIUM DIBORIDE SUPERCONDUCTOR

3.1 MgB_2 Breakthrough

The discovery of superconductivity in MgB_2 has been announced by Japanese researchers in 2001 (17) in a paper published in the journal Nature, titled "Superconductivity at 39 K in magnesium diboride". The team was led by Jun Akimitsu, a physicist at Aoyama Gakuin University, who discovered the superconducting properties of MgB_2 while investigating the properties of a new class of compounds called "borocarbides." The team found that a sample of MgB_2 had a superconducting transition temperature of 39 K as shown in Figure 3.1, which was much higher than the transition temperatures of other known binary superconductors at the time. The discovery of MgB_2 as a superconductor opened up new possibilities for the use of high-temperature superconductors in a wide range of applications and has led to significant research efforts in the field of superconductivity.

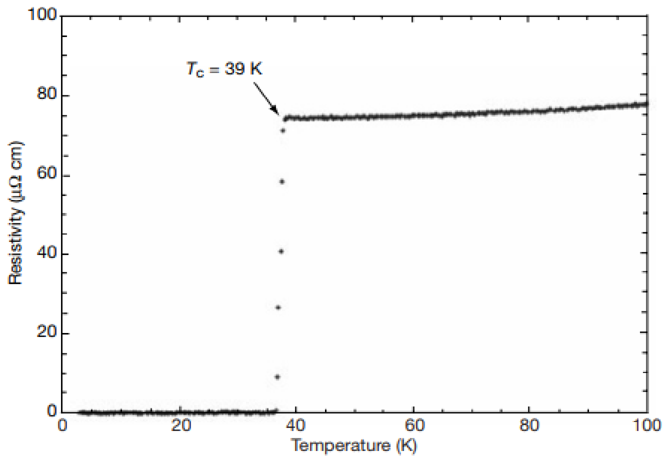

Figure 3.1. Temperature dependence of the resistivity of MgB_2 under zero magnetic field (17).

3.2 Lattice Structure of MgB_2

MgB_2 has a hexagonal crystal structure, also known as the AlB2-type structure and the lattice parameters are a = b = 3.086 Å and c = 3.522 Å (17). The crystal structure of MgB_2 is composed of layers of boron atoms stacked on top of each other, boron atoms are arranged in graphite-like honeycomb planes that are separated by hexagonal layers of magnesium atoms, as depicted in Figure 3.2. The crystal structure of MgB_2 can be described as follows:

1. The B atoms form a hexagonal lattice in each layer.
2. The Mg atoms occupy the sites between the layers, forming a hexagonal close-packed (HCP) arrangement.
3. The Mg atoms form covalent bonds with the B atoms in the adjacent layers, creating a three-dimensional network of B-Mg-B bonds.

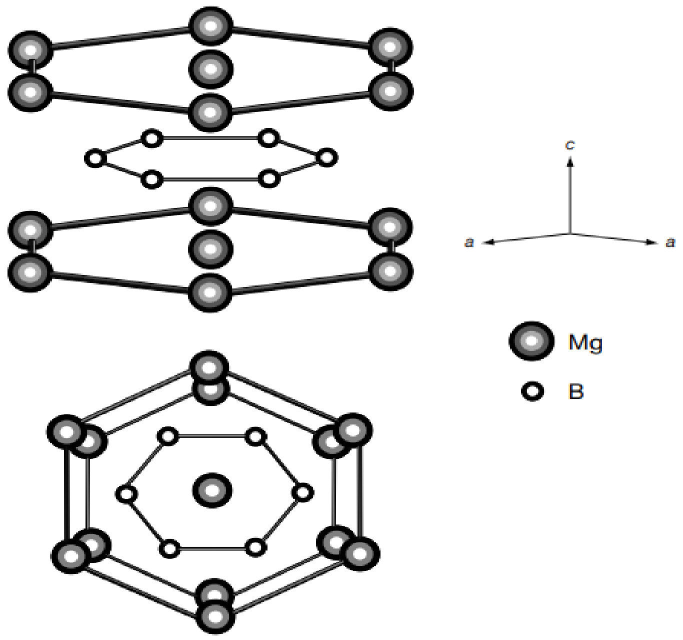

Figure 3.2. Crystal structure of MgB_2 (17).

The distance between boron atoms is shorter in the ab-plane than in the c-direction, with a B-B layer distance of 1.780Å and an Mg-Mg layer distance of 3.084Å. Its crystal structure shows anisotropy in the interatomic distances between B-B atoms because of its hexagonal structure and relatively the longer distance between boron planes than boron atoms. MgB_2 exhibits superconductivity with a high transition temperature due to strong electron-phonon interactions. The high vibrational frequencies of the light B atoms in MgB_2 facilitate these interactions, resulting in a higher critical temperature compared to other inter-metallic compounds (24).

3.3 Electronic Configuration of MgB_2

The superconductivity in MgB_2 is due to the presence of two types of electron bands, which are three dimensional π-bands and two dimensional σ-bands. The 2-Dimensional σ-bands are mainly formed by the overlap of in-plane B-B bonds, while the P_z orbitals of the boron planes give rise to the 3-Dimensional π-bands (25). The π-band in MgB_2 consists of both holes and electrons as charge carriers. In the crystal structure of MgB_2, magnesium and boron atoms form an ionic bond, with magnesium atoms donating their valence electrons to the boron layer and becoming fully ionized (26). At the Fermi level of MgB_2, the electrons are mainly p-electrons (electrons that occupy the p orbitals) of boron along with magnesium donating s-electrons (electrons that occupy the s orbitals) to the conducting bands (27).

The Fermi surface of MgB_2 is mainly derived from the boron orbitals, as the boron bands are more effective in the formation of valence bands than the magnesium bands. Many researchers have proposed that the metallic boron layers, which has been observed by charge density distribution (28), play a significant role in the superconducting properties of MgB_2 (29). Upon examination of the density of states (DOS) and band structure of MgB_2, it is observed that there is a major transfer of electrons from the Mg atom to the two B atoms. The p-orbital contribution of Boron atoms is dominant on the overall shape of the total DOS (30). Additionally, electronic structure calculations demonstrate that, despite the weak bonding between magnesium atoms, there is a strong covalent bond between boron atoms, leading to a strong electron-phonon interaction.

3.4 Energy Gap Symmetry of MgB_2

The superconducting energy gap have influences on the properties of a superconductor.The superconducting energy gap have influences on the properties of a superconductor. In the case of conventional superconductors, the superconducting gaps are isotropic while for the high temperature superconductors the superconducting gaps are anisotropic (31). S-wave superconductors have a superconducting gap which is isotropic, whereas d-wave superconductors have a superconducting gap which is anisotropic. Over the Fermi surface of MgB_2, the phase of the gap does not change, indicating that MgB_2 is an s-wave superconductor (32).

3.4.1 Explaination of Two Gap Superconductivity

The mechanism of superconductivity in MgB_2 is still under debate, but it is widely accepted that it involves two distinct energy gap, rather than the single energy gap typically found in conventional superconductors. Figure 3.3 shows that the presence of these two gaps has been observed in various experiments including angle-resolved photoemission spectroscopy (ARPES) and tunnelling measurements (33). Two band gaps in MgB_2 were first estimated by Choi (25). The larger band gap σ is 6.8 meV and smaller band gap π is 1.8 meV. The first gap, which is smaller and located near the Fermi level, is associated with the in-plane bonding boron atoms and is believed to be responsible for the s-wave pairing state. This gap is thought to be caused by electron-phonon interactions, with the phonons in MgB_2 being responsible for the pairing. The phonon frequency at the zone centre is found to be relatively high and are found to be responsible for the high T_c of MgB_2 (29).

The second gap, which is larger and located farther from the Fermi level, is associated with the out-of-plane boron atoms and is believed to be responsible for the d-wave pairing state. This gap is thought to be caused by electronic interactions between the boron and magnesium atoms. The electronic interactions between out-of-plane boron atoms and Mg atoms are believed to be responsible for the d-wave pairing (29). The presence of two gaps in MgB_2 is thought to contribute to its relatively high superconducting transition temperature T_c of 39 K, as well as its high critical magnetic field.

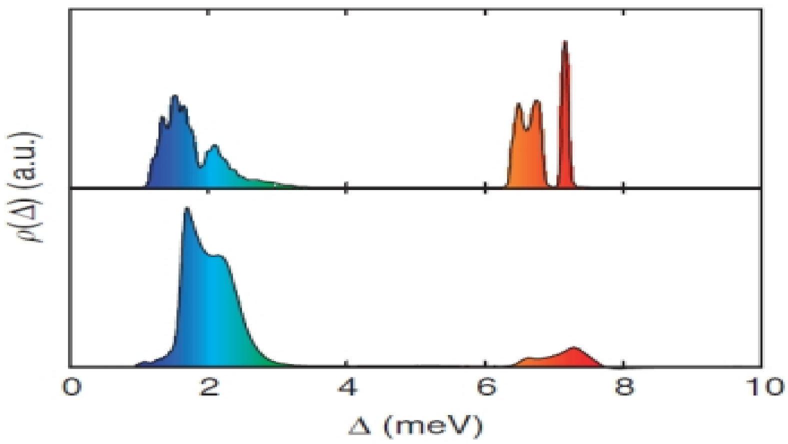

Figure 3.3. Two band structure from theory (Top) and tunnelling spectrum (Bottom) (33).

3.5 Anisotropy γ

Anisotropy refers to the phenomenon where the electrical and magnetic properties of the material depend on the crystal orientation. The anisotropy of MgB_2 is 1.5 – 5, which is comparatively lower than HTS having 50 – 200 (18). The crystal structure of MgB_2 causes its electromagnetic properties to exhibit anisotropy, with a longer coherence length in the a-b plane compared to the c-axis (26). As a result, when the magnetic field is applied along the c-axis perpendicular to the plane, the upper critical field has a lower value, as shown in Figure 3.4.

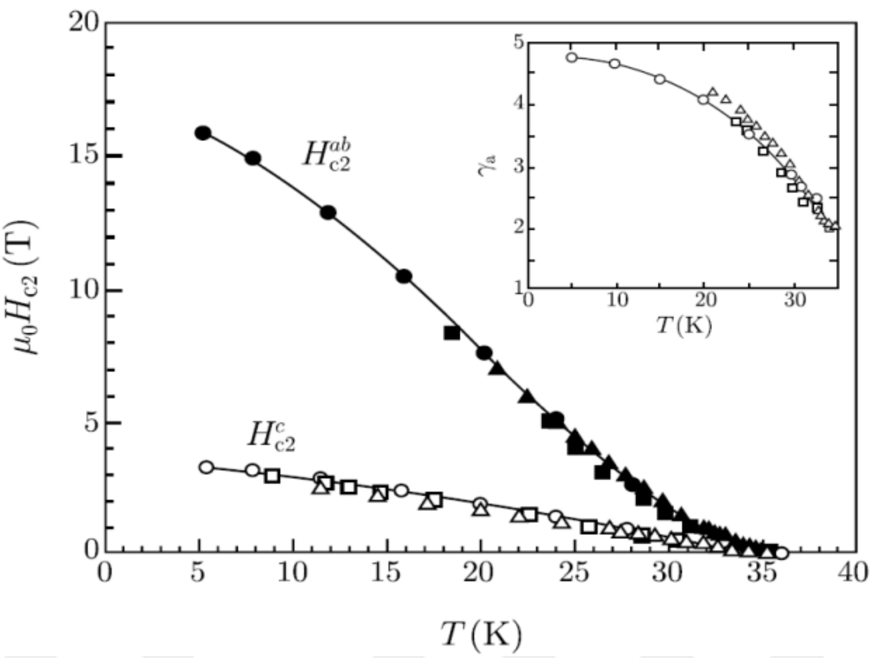

Figure 3.4. The temperature dependence of the upper critical field in a single crystal of MgB_2, the inset represents the anisotropy γ_a of the upper critical field (34).

In Figure 3.4, the mathematical expression of anisotropy γ_a for upper critical field is represented by Equation (3.1)

$$\gamma_a = H_{c2}^{ab} / H_{c2}^{c} \tag{3.1}$$

The coherence lengths calculated from the upper critical fields are approximately $\xi_c(0) = 9.6$ nm and $\xi_{ab}(0) = 2.0$ nm.

3.6 Isotope Substitution Effect

In 1950, isotopic substitution effect for mercury was conducted by two different laboratories, Renolds et al (4) at Rutgers university and at National Bureau of Standards (5) known as isotope effect. The isotope effect for MgB_2 refers to the phenomenon in which the superconducting properties of the material are affected by the isotopes of the constituent elements. Isotope effect indicates that the superconductivity is phonon mediated. Specifically, it has been observed that replacing the isotope of Mg with a heavier isotope can lead to an increase in the critical temperature T_c. The isotope effect is represented by the relation $T_c \propto M^{\alpha}$

where M is atomic mass of element. The isotope effect α for some element is shown in Table 3.1.

Table 3.1. Isotope effect for some elements (35).

Element	Isotope Effect α
Mg	0.5
Sn	0.46
Mo	0.33
Re	0.4
Zr	0 (±0.05)

It has been observed that $Mg^{10}B_2$ and $Mg^{11}B_2$ showed the existence of boron isotope effect with coefficient of α= 0.26 ±0.03 and 1K shift at critical temperature T_c (36). The isotope effect is related to the change in the phonon spectrum and this provided evidence that MgB_2 exhibits BCS superconductivity.

3.7 Effective Grain Connectivity

Grain connectivity, porosity and weak link are related to the microstructure of the superconducting material and can impact its superconducting properties. It has been estimated that the grain size changes between 10nm to 200nm in MgB_2 (37). Grain connectivity refers to the degree to which the grains in a sample of MgB_2 are connected to one another. A higher degree of grain connectivity is associated with a higher critical current density J_c in MgB_2 (38). This is because a higher degree of grain connectivity leads to a more homogeneous distribution of the superconducting current throughout the material, which reduces the number of weak links and improves the overall superconducting properties.

In contrast to high-T_c superconductors, the weak link problem is almost absent in MgB_2 (39). The natural grain boundaries are regarded as the source of pinning centres in MgB_2 superconductors.

Porosity refers to the presence of voids or empty spaces within a sample of MgB_2 and it is always present due to volume shrinkage caused by the reaction of

Mg with B for an in-situ processed MgB_2 sample. During the reaction between Mg and B, there is a volume contraction that reduces the density of the ceramic core of the wire and the final mass density of the wire core is about 50% of the theoretical density of pure MgB_2 (40).These voids and empty spaces act as barriers to the flow of superconducting currents and can reduce the overall connectivity of the grains.

3.8 MgB_2 Phase Formation

MgB_2 is achieved by the reaction between boron and magnesium elements at specific temperature. In Figure 3.5, the process of phase formation is illustrated with Differential Thermal Analysis (DTA) measurement. The occurrence of two reactions is indicated by the presence of two peaks in the DTA curve, as depicted below.

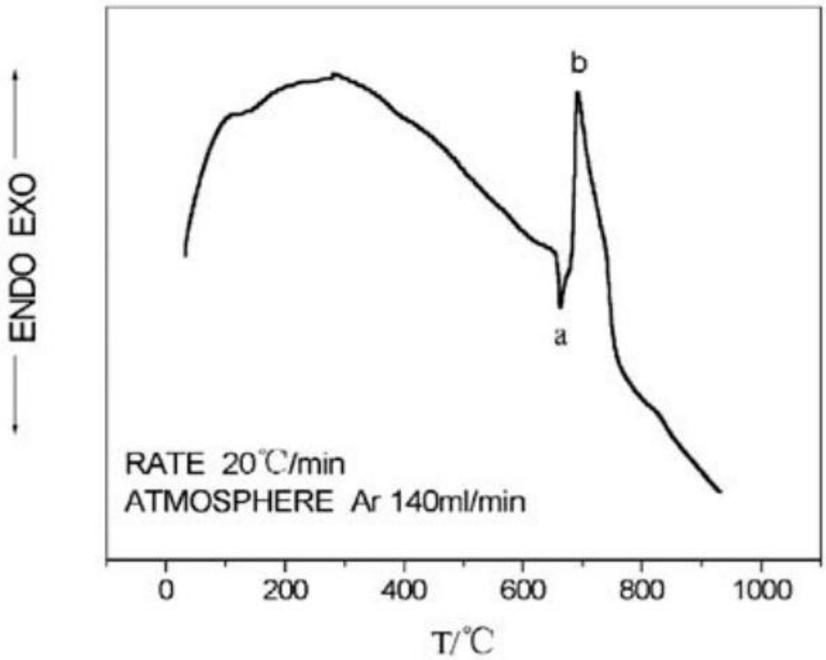

Figure 3.5. Differential Thermal Analysis (DTA) curve for the mixture of Mg:B in a ratio of 1:2 (41).

$$Mg\ (S)\ \overset{a}{\rightarrow}\ Mg\ (L) \tag{3.2}$$

$$Mg\ (L) + 2B\ (S)\ \overset{b}{\rightarrow}\ MgB_2\ (S) \tag{3.3}$$

In the above equations, 'S' and 'L' denote the solid and liquid phases, respectively. Reaction (a) indicates the transition of Mg from a solid to a liquid state, whereas Reaction (b) signifies the formation of the MgB_2 phase. It is evident that the formation of MgB_2 in Equation (3.3) occurs immediately after the melting of Mg in Equation (3.2), and this reaction proceeds rapidly. The vapour pressure at the melting point of Mg (650°C) is only 135 Pa, indicating that the evaporation of Mg at this temperature is minimal (41).

The growth and formation of MgB_2 phase can be defined in three-step process:

1. Firstly, there is rapid infiltration of Mg into surrounding boron and then melting of remaining magnesium into liquid. Highly dense B layer can suppress the Mg infiltration.
2. Secondly, magnesium reacts with boron. As heat-treatment proceeds, more and more B particles transform into MgB_2 grains which continue to grow and merge together. As molar volume of B (4.59 $cm^3\ mol^{-1}$) is four times smaller than that of MgB_2 (17.46 $cm^3\ mol^{-1}$) (42), so MgB_2 reaction fills up the gap between initial Boron particles. As a result, 100% dense MgB_2 layer is formed close to surface of prior Mg which prevents further infiltration of Mg into B particles.
3. Finally, Mg have to diffuse through dense MgB_2 layer to react with remaining B particles, which is slower than previous steps (43). The schematic diagram of reaction between magnesium and boron is shown in figure 3.6, Mg (S) and Mg (L) represents Mg-rich solid and liquid phases, also B (S) represents solid phase of boron.

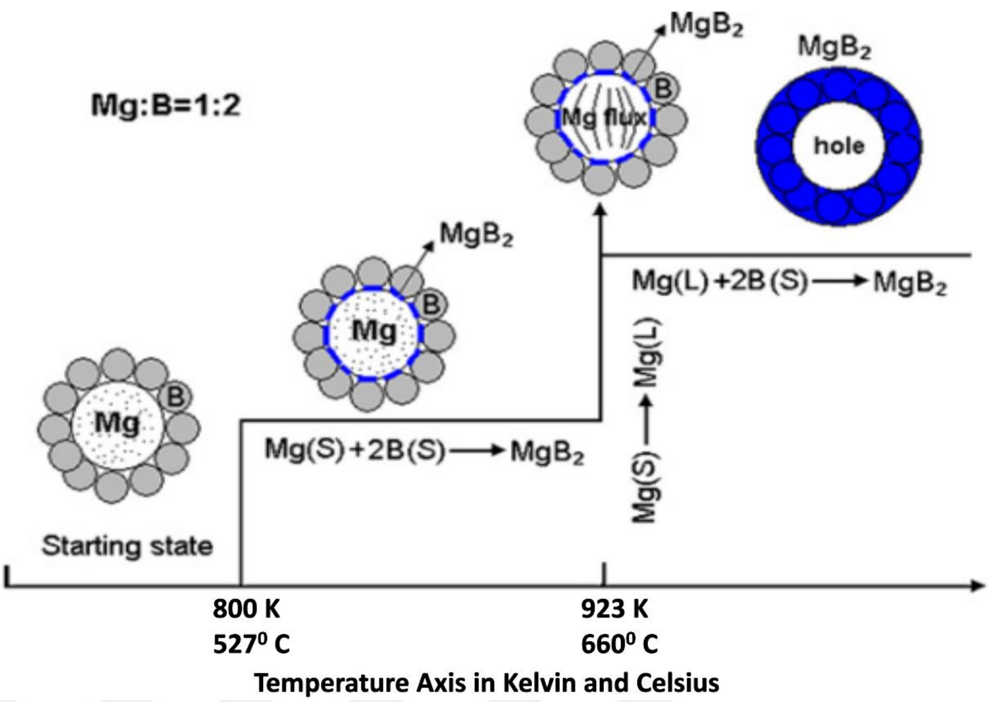

Figure 3.6. Schematic model for MgB_2 formation (44).

4. WIRE PRODUCTION TECHNIQUES

There are various techniques for the fabrication of MgB_2 wires and tapes. Every technique has its advantages and disadvantages over other techniques but the main goal is to enhance superconducting properties which are affected by fabrication techniques. Current transport capability (critical current density, $J_{c,B}$) in a magnetic field is the most crucial characteristic of superconducting wires for practical applications. For fabrication, most reliable in-situ techniques are Powder-In-Tube (PIT) (45), Continuous Tube Filling and Forming (CTFF) (46) and Internal Magnesium Diffusion (47).

4.1 Powder in Tube Technique

To fabricate MgB_2 wire using Powder in Tube (PIT) technique, one end of a pre-cleaned metallic tube is first closed using an appropriate plug material such as aluminium or lead etc. by squeezing. The empty tube is then filled with the powder mixture, MgB_2 or Mg + 2B. Finally, the open end of the filled tube is closed using the same material as the other closed end, and the metallic tube is ready to be deformed into a wire as shown in Figure 4.1. If the precursor powder is reacted before filling into metal tube, then this process is called ex-situ. On the other hand, if filled powder is not reacted then it is called in-situ method.

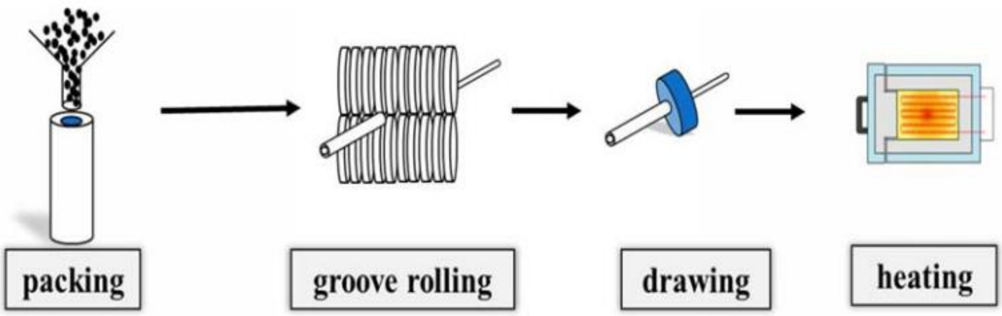

Figure 4.1. PIT technique for fabrication of wires (48).

PIT is the most common technique for the fabrication of MgB_2 wires but the J_c is relatively lower compared to other fabrication technique such as IMD, primarily due to reduced connectivity. The J_c of MgB_2 can be improved by using high purity of Mg and B powders.

4.2 CTFF Technique

Hyper Tech uses a patented process for manufacturing MgB_2 wires (46) and this process is called the continuous tube filling and forming (CTFF) as shown in Figure 4.2, a quick MgB_2 wire fabrication method. A continuous metal strip of niobium Nb is used as inner barrier in this method. It gradually deformed into 'U' shape as this metal ribbon passes through the tube forming dies. Then, the mixture of Mg and B powders is poured into a metal strip shaped like 'U'. The tube is then sealed using closing dies. To provide additional protection, the filled tube is inserted into another tube, and the combined tubes pass through a series of dies to reduce the diameter and achieve the desired final shape. Similar to PIT method, it has also connectivity problems. On the other hand, IMD method ensures better connectivity. CTFF technique enables the rapid production and allows for the fabrication of longer lengths of wires in comparison to other fabrication techniques but CTFF method is not promising to obtain highly dense and compressed precursor powders.

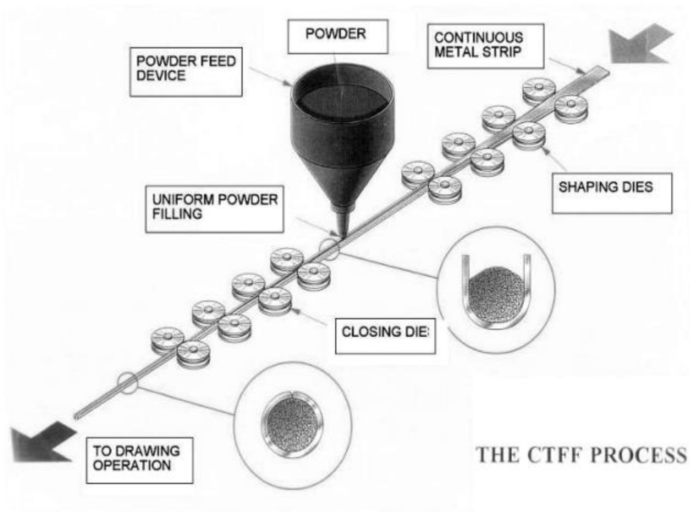

Figure 4.2. Schematic view of CTFF Method (49).

4.3 IMD Method

A new fabrication technique was introduced by Giunchi et al. (47) in which a uniform Mg rod was placed into the centre of metallic tube and then gap was filled by boron powder as shown in Figure 4.3. High J_c can be achieved by using IMD (Internal Magnesium Diffusion) technique. Disadvantage of using the IMD method is that it can result in the formation of a hole at the center of the wire. This occurs because the infiltration of Mg into the B material creates a gap existance of which reduces the engineering critical current density J_{ce} of the wire. J_{ce} is calculated by dividing the critical current I_c to the total cross-sectional area of the wire. The optimal precursor B powder and selection of effectual additives resulted in the fabrication of high J_c second generation MgB_2 wires by using IMD technique (50). Due to its high performance, still research is going on for the production of long wires by using IMD method (51).

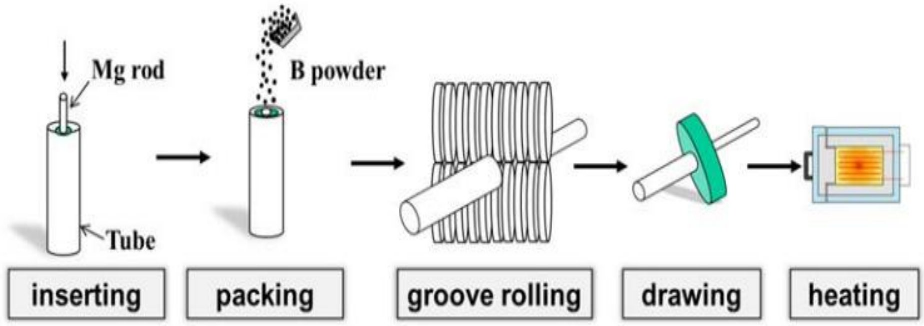

Figure 4.3. Fabrication Process for IMD wires (48).

4.3.1 Standard IMD Technique

In Standard IMD technique, Mg rod is placed in the middle of tube and rest of tube is filled with boron as shown in Figure 4.3. By using this technique, sometimes Mg does not fully diffuse into boron, and the presence of un-reacted Mg and an un-reacted boron layer close to the sheath region suppresses the superconducting properties.

4.3.2 Powder IMD Technique

For the Powder IMD, all process is same as standard IMD but Mg powder is used instead of Mg rod in this technique. One benefit of using magnesium powder in the centre is that it facilitates complete diffusion of magnesium due to its faster diffusion rate in powder form (52). The reaction rate is typically faster in a powdered solid compared to an equivalent mass present as a single lump. This is due to the powdered solid having a larger surface area than the single lump. Compared to using magnesium rod, the use of magnesium powder is more advantageous as it allows for greater control over the size of the magnesium particles and the Mg/B ratio. This is particularly important as magnesium rods are not available in all sizes.

4.4 HIP and CHPD Techniques

Mostly, in-situ PIT processed MgB_2 wires possess porosity and weak connectivity between grains of MgB_2, which can be overcome by using IMD method, but porosity still occurs because of Mg reaction with B. During the reaction between Mg and B, there is a volume contraction that reduces the density of the ceramic core of the wire and the final mass density of the wire core is about 50% of the theoretical density of pure MgB_2 (40).

The densification of the core of PIT MgB_2 wires has been extensively studied with regards to grain connectivity and porous structure. The Hot Isostatic Pressure (HIP) method (53), which uses high pressure to complete the reaction, can significantly increase the density of the MgB_2 core, but is only applicable to short wire samples. Conversely, the Cold High Pressure Densification (CHPD) method can be used at longer length scales (54) and can produce a denser starting Mg+2B in-situ wire core than the conventional in-situ PIT method. However, it is not as effective in improving core density and reducing porosity as the HIP process. The schematics of HIP is shown in Figure 4.4.

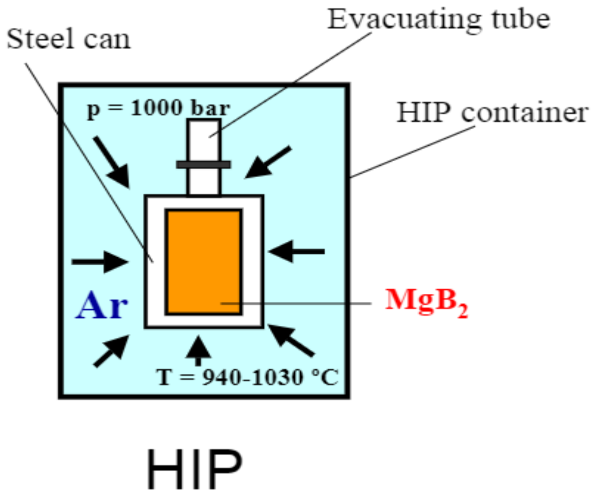

Figure 4.4. Schematics of Hot Isostatic Pressing (55).

4.5 Dopping Effects on the Superconductivity of MgB_2

Several techniques have been introduced to enhance the J_c of MgB_2, including chemical doping, thermo-mechanical processing, ball milling and proton irradiation. Among these methods, chemical doping has been found to be the most effective approach to improve the superconducting properties of MgB_2. Doping enhances the J_c while concurrently suppressing the growth of the MgB_2 layer by acting as a barrier during infiltration of Mg.

Various elements such as Al and C, and various compounds such as SiC and hydrocarbons have been used as dopants to enhance the critical current properties of MgB_2 (56). In SiC-doped MgB_2 bulk, both silicon Si and carbon C are believed to contribute to the improvement of H_{irr} and J_c by substituting at the boron B site. It has been reported that the small amounts of carbon and aluminium (up to 2.5%) as dopants can increase the J_c by a factor of 2, while keeping the T_c unchanged (57).

When carbon is used as a dopant, the carbon atoms that remain at the grain boundary or interstitial sites can serve as pinning centres for vortices, leading to extrinsic pinning and hence helps in enhancing the H_{c2}, H_{irr}, and J_c values (58). Fine powders of Y_2O_3 (59), SiO_2 (60), and metal carbonates (61) like Li_2CO_3, Na_2CO_3 and Mg_2CO_3 have also been found to be effective dopants for enhancing J_c.

4.6 The Sheath Material

The sheath material plays an important role in the fabrication of MgB_2 wires, as it serves as a protective layer for the superconducting material inside the wire. The selection of a sheath material for MgB_2 wires is important for following reasons:

1. Mg/B is a reactive material that can easily oxidize in air, leading to a loss in superconducting properties. A suitable sheath material can protect the MgB_2 wire from oxidation and maintain its superconducting properties.
2. MgB_2 wires can be brittle and fragile, and a suitable sheath material can provide mechanical support and protection against mechanical stress.

Examples of sheath materials that have been used for MgB_2 wires are Iron (Fe), Stainless Steel (SS), Nickel (Ni), Copper (Cu), Silver (Ag) and Niobium (Nb). All of them have advantages and disadvantages over each other. Stainless steel and niobium are difficult to machine and silver, niobium are expensive. Copper is ductile but the higher rate of reaction with Mg is an obstacle and at the same time the softness of the copper metal as sheath material is a disadvantage for wire drawing. The use of Iron as a chemical barrier lowers the initial cost for in-situ wires, but there are highly chances of B diffusion into Fe sheath (62).

4.7 Cold Drawing

Cold drawing is a process in which a material is deformed at room temperature passing it through a die by mechanical pulling. During this process, compression stresses and tensile stresses occur, causing the elongation of material. Figure 4.5 represents the schematic structure and 3-D view of die set.

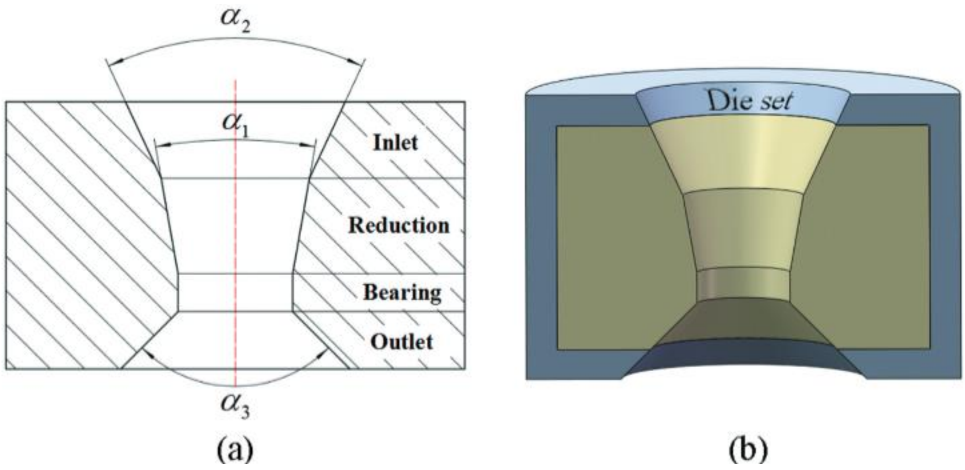

Figure 4.5. The standard drawing die: (a) The schematic structure; (b) The 3-D model with a die set (63).

A standard wire drawing die typically consists of four segments, as depicted in Figure 4.5. The first segment, known as the inlet (or entry zone), plays a role in facilitating the entry of billets and the formation of lubricant films. Subsequent to the inlet is the reduction zone (or drawing zone), which serves as compacting the lubricants to create a denser lubricant film and inducing plastic deformation to decrease the diameter of the billets. The bearing section (or calibration zone) that follows the reduction zone is used to calibrate the final diameter and refine the surface profile. Ultimately, the primary function of wire drawing is accomplished by the end of this process (63).

Cold drawing can have several effects on the material's properties, depending on the specific material and the conditions of the process. Some of the main effects of cold drawing on a material include:

1. Cold drawing can effect the strength and ductility of a material. By applying a tensile stress to the material, the dislocations within the material become more densely packed, which makes the material stronger and more resistant to further deformation.
2. Cold drawing can also improve the microstructure of a material by aligning the grains in the direction of the elongation. This improves the overall mechanical properties of the material until a certain total reduction ratio is reached.

During cold drawing, there is possibility of wire defects known as the wire break, internal crack and surface crack as shown in Figure 4.6. The optimization of die angle and reduction per pass are important factors for the prevention of defects. Usually defects happens because of difference of tensile stress and compression stress during cold drawing, and wire break occurs when internal tensile stress increases up to maximum tensile strength (64).

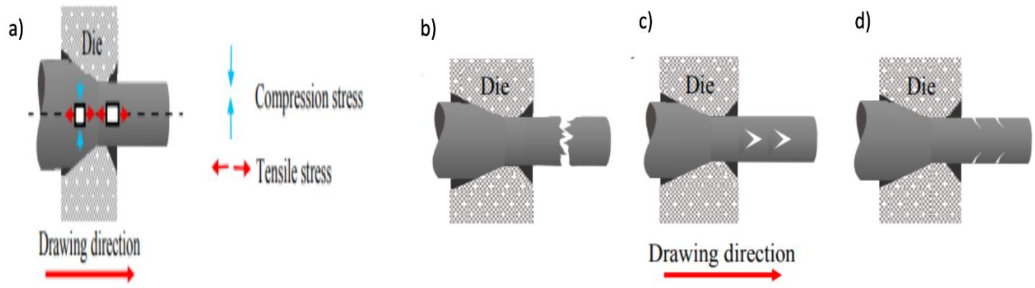

Figure 4.6. During cold drawing: (a) Occurrence of stresses; (b) Wire break; (c) Internal Crack; (d) Surface Crack (64).

4.7.1 Work Softening Behaviour of Mg

Mostly, deformation does work hardening. Usually, the strength and hardness of all alloys and Mg-alloys increases during cold drawing but magnesium shows work softening behaviour at a particular level of strain. There are dislocations during deformation and accumulation of dislocations causes hardening of material. Heat treatment is required to get rid of dislocations. During cold drawing of Mg rod, initially there is rapid increase in hardness and strength, and then it shows work softening behaviour. It can be attributed to dynamic recovery and recrystallization of pure Mg at room temperature during cold drawing (65).

Susner et al. (66) investigated the effect of elongated-Mg particles during cold drawing, shown in Figure 4.7, and heat treatment time on the superconducting properties of PIT in-situ processed MgB_2 strands. During the heat treatment process, the Mg in the wire forms a fibrous macrostructure of MgB_2 as it reacts with the B powder. This reaction leaves behind long voids, resulting in fibres or veins that are approximately 20 μm long and 2.5 μm across (the macrostructure), comprise a collection of grains that are randomly oriented, relatively well connected fine polycrystalline MgB_2 grains typically 50 nm in size (66). Within the strand, the veins of polycrystalline MgB_2 are preferentially oriented longitudinally and the electrical connectivity between them differs in the transverse and longitudinal directions. Hence, poor connectivity causes the large difference between the longitudinal and transverse critical current densities.

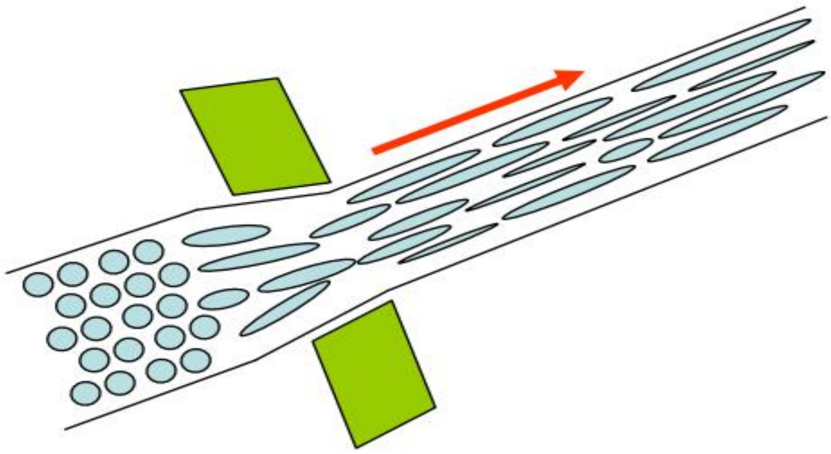

Figure 4.7. Conceptualization of Mg elongation during wire drawing process (66).

4.8 The Potential of MgB_2 Superconductor

The MgB_2 superconductor has attracted significant attention due to its potential in various technological applications. Its low cost and several intrinsic properties, such as low mass density, low anisotropy, high critical current density and high critical temperature (T_c = 39K), make it advantageous over conventional superconductors. Enormous research has been done to enhance J_c of MgB_2 in order to enable it to replace conventional superconductors. By using the method of CHPD, the relative mass density inside MgB_2 filaments of in-situ mono and multifilament wires were increased from 40% to 60% by pressure above 1 GPa, which in result enhanced the J_c strongly (67).

The best physical J_c of MgB_2 monofilament wire with 3 mol% C, by using the advanced internal Mg infiltration method (AIMI), has been reported to be 1.5×10^5 $A.cm^{-2}$ under 9.5T at 4.2K (68). In case of IMD method, there are significant limitations in terms of filling factor, mechanical strength and reliability. Still, MgB_2 has several potential advantages over other superconductors, which make it an attractive candidate for various applications. Here are some of the superiorities of the MgB_2 superconductor:

1. The critical temperature T_c of MgB_2 is around 39K, which is higher than conventional superconductors like Nb_3Sn, NbTi, and Pb. This makes MgB_2 more suitable for superconducting applications at higher cryogenic temperatures.
2. For practical applications, MgB_2 can operate at temperatures in the range of 10-30K, and modern cryocooler systems can achieve this temperature range.
3. MgB_2 has a relatively low anisotropy compared to other superconductors, which means that it is easier to manufacture wires and tapes of this superconductor. This makes it more suitable for large-scale applications like power transmission.
4. MgB_2 is made of low-cost materials, magnesium and boron, which are abundant and inexpensive. This makes it a cost-effective alternative to other high-temperature superconductors like $YBa_2Cu_3O_7$ (YBCO).
5. Potential applications for MgB_2 superconductors can be MRI machines (69), the superconducting Wind Turbines (70), Fault Current Limiters (71) and electrical power transformers (72).

5. EXPERIMENTAL WORK

In this part of the thesis, the whole experimental setup is discussed. Preparation of samples and various experiments were performed to study the superconducting and mechanical behaviour of MgB_2 wires.

5.1 Fabrication of Standard and Powder IMD Wires

Two wires were fabricated using standard and powder IMD techniques. For both types of wires, an iron tube was used as sheath material.

5.1.1 Powder IMD Wire

For the fabrication of powder IMD wire, we used 15 cm long iron tube. Outer diameter of iron tube was 12 mm and inner diameter was 9 mm. After cleaning the iron tube with ethyl alcohol, one end of iron tube was sealed with aluminium with the length of 7.5 cm. Then the guide rod (copper rod) was placed in the middle of iron tube and filled the remaining space with boron powder. Boron powder that was used for filling was 98% pure. The diameter of guide rod (copper rod) was 6mm. After filling with boron, the guide rod was removed carefully without damaging the surrounding Boron layer. After successfully removing the guide rod, the central bore region was filled with Magnesium powder. The Mg powder that was used for the filling process was 99% pure. Finally, the iron tube was sealed with aluminium having length of 1.5 cm.

5.1.2 Standard IMD Wire

We used a 12 cm long iron tube to prepare a standard IMD wire. Inner and outer diameters of this iron tube were again 9 mm and 12 mm, respectively. Iron tube was cleaned thoroughly, then one end of iron tube was sealed with aluminium and the filling length of aluminium was 6 cm. Then magnesium rod was placed in the middle of iron tube and remaining space was filled with boron. For this process, it was important to keep the magnesium rod in the middle region. The diameter of Mg rod was 4.66 mm. After filling the boron completely, the end of iron tube was sealed with aluminium.

5.2 Cold Drawing

For the deformation of filled iron tube until desired diameter, cold drawing steps were performed. The outer diameter of the iron tube was 12 mm at the beginning and cold drawing steps were performed until the outer diameter of the wire sample was reduced to 1.08mm diameter. Dies were applied in such manner that for every pass there was area reduction between 5 and 10 percent. After every 30% reduction of diameter, intermediate heat treatment was applied to the wire in the furnace.

$$R_t = \frac{D_f}{D_i} \times 100\ [\%] \qquad (5.1)$$

The Equation (5.1) was used to calculate the percentage of total reduction in diameter, D_i is diameter before drawing and D_f is diameter after drawing.

Table 5.1. Cold drawing steps for powder and standard IMD wires.

Starting Diameter	Diameter after Drawing	Total reduction %	Intermediate Annealing	Drawing speed	Die Material
12 mm	8.4 mm	30	300°C for 2h	39 cm/min	Tungsten Carbide
8.4 mm	5.8 mm	30	300°C for 2h	39 cm/min	Tungsten Carbide
5.8 mm	4.1 mm	30	300°C for 2h	39 cm/min	Tungsten Carbide
4.1 mm	2.8 mm	30	300°C for 2h	39 cm/min	Tungsten Carbide
2.8 mm	2.0 mm	30	300°C for 2h	39 cm/min	Tungsten Carbide
2.0 mm	1.4 mm	30	300°C for 2h	39 cm/min	Tungsten Carbide
1.4 mm	0.9 mm	30	300°C for 2h	39 cm/min	Tungsten Carbide

5.2.1 Intermediate Heat Treatment

During cold drawing, intermediate annealing was applied to standard and powder IMD wires for 2 hours after every 30% reduction of diameter at 300°C and intermediate annealing of deformed Mg at 300°C shows better mechanical properties (73) . A long furnace was used for intermediate annealing of wires. Work hardening is caused due to plastic deformations during cold drawing. The cold drawing process induces excessive stresses in the microstructure of the cold drawn wire and the induced excessive stress causes non-uniformity, which effects mechanical properties of material. For that reason, intermediate heat treatment is necessary after a few steps of cold drawing process because it improves the microstructure of wire by promoting a recovery, recrystallization of grain structure and reducing the presence of defects. So, this process causes the material to return to a more ductile state by mitigating the negative effects of work hardening.

5.2.2 Mechanical Behaviour of Mg

During cold drawing of standard IMD wire, mechanical behaviour of Mg is important because Mg rod is used for the fabrication of standard IMD wires, so uniformity of Mg in the core of wire is very important for superconducting properties. Cold drawing induces mechanical deformation, leading to work hardening and dislocation accumulation. To maintain the strength and elongation properties of Mg during cold drawing, it is crucial to perform intermediate annealing after reducing a specific amount of cross sectional area. According to Meng et al. (73) intermediate annealing at 300ºC for 30 minutes of deformed Mg shows better mechanical properties, as shown in Figure 5.1.

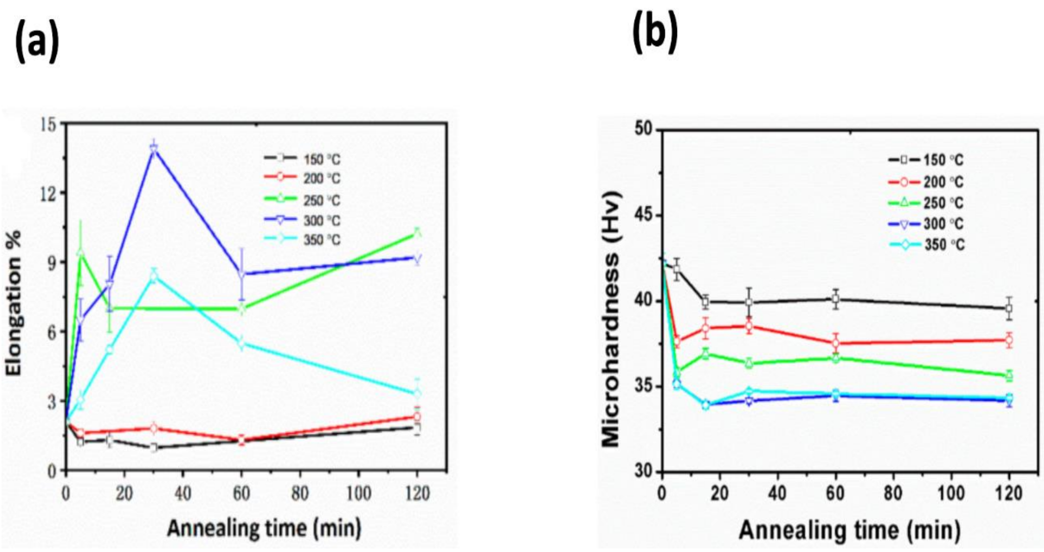

Figure 5.1. (a) Elongation of pure Mg during tensile tests with different annealing treatments (73) and (b) microhardness of Mg with different annealing treatments (73).

5.3 Final Heat Treatment

The final heat treatment for the formation of the MgB_2 phase in wires was carried out at a temperature of 650°C for a duration of 1 hour. The tube inside the cylindrical furnace was cleansed by vacuum pumping and argon filling process. After cleaning process, the heat treatment was performed in the presence of 5-10 bars of Argon gas pressure for the prevention of oxidation.

5.4 Vickers Hardness

The powder IMD and standard IMD wires are two different techniques so there could be a possibility of having different strengths for different layers after cold drawing. To observe miscrohardness of different regions, Vickers Hardness tests were performed. Firstly, samples were moulded by using phenolic resin. After making the mould, the samples were polished carefully so that three regions (Iron, Boron and Magnesium) became clearly visible. Total 18 samples were produced for HV measurements. The Equation (5.2) was used to calculate HV value.

$$HV = 0.1891\ \frac{F}{d^2}[N/mm^2] \tag{5.2}$$

In above formula, F is the applied force in newtons (N) and d is diagonal distance (mm). The indentation mark or trace left behind because of diamond is shown in Figure 5.2.

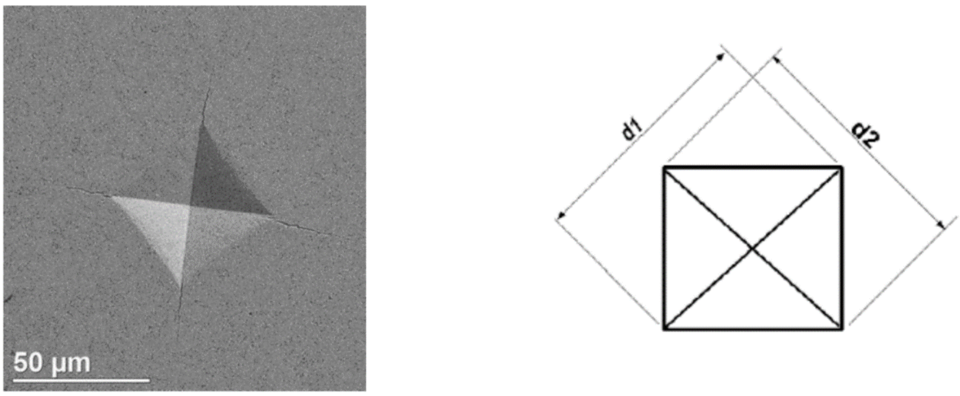

Figure 5.2. Indentation trace and diagonals of trace (74).

5.5 Transport Current Measurement Technique

The electrical properties of MgB_2/Fe wires were examined through resistance-temperature (R-T) and current-voltage (I-V) measurements. The closed-cycle helium cryostat system was used to perform the transport experiments. When using this system, maximum 1 A dc current can be applied and performed measurements with an applied field of up to 7T. The samples were placed in the cryostat in such a way that they were perpendicular to the magnetic field and the system was cooled in a zero magnetic field (ZFC). To measure temperature dependent sample resistance, a 50 mA direct current (DC) was applied in the temperature range of 20K to 45K by using four probe method.

6. RESULTS AND DISCUSSION

In this thesis, the detailed fabrication processes and measurement results for Powder IMD wire and Standard IMD wire were presented and discussed. Various experimental works which were performed to observe the superconducting and mechanical properties of Powder and Standard IMD wires such as Temperature-dependent resistivity measurements, in-field current-voltage measurements and Vickers Hardness measurements are discussed below.

6.1 The ρ-T Curves

The temperature dependent resistivity curves of Powder and Standard IMD wires in a zero magnetic field are shown in Figure 6.1. Both samples were heat treated at 650°C for 1 hour. The resistivity measurements of superconducting wires were performed on the round wires with outer diameters of 1.08mm by applying 50mA dc transport current.

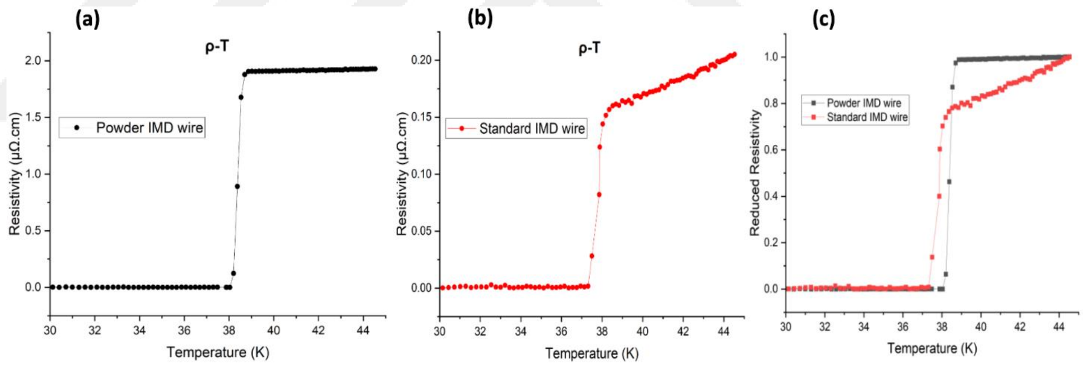

Figure 6.1. Temperature dependent resistivity curves of (a) powder IMD wire, (b) standard IMD wire and (c) reduced resistivity for powder and standard IMD wires.

The resistivity for both wires is less than 2 μΩ.cm and there is 10 times difference between resistivity of samples at 45K. Powder IMD sample showing better superconducting behaviour than standard IMD sample in terms of critical transition temperature. For powder IMD sample, at transition, the resistivity is nearly 2 μΩ.cm while for standard IMD sample, at transition, the resistivity is nearly 0.15 μΩ.cm. There is one order of magnitude difference and it can be referred to the presence of the un-reacted Mg in standard IMD wire sample. The slope of ρ-T curves above 40K is indicative of the grain connectivity in the core region. The low slope observed in the ρ-T curve of powder IMD wire above 40K suggests that the grains in the core region of are well connected than the grain connectivity in the core of standard IMD wire.

Furthermore, powder IMD wires showed better superconducting properties than standard IMD wire. There was an un-reacted Mg layer in standard IMD wire that caused transition in standard IMD wire at lower zero resistivity temperature than powder IMD wire. The T_c 37.5K of standard IMD wire was also lower than the T_c 38.3K of powder IMD wire. Also the transition for powder IMD sample was sharper than standard IMD sample.

6.1.1 Optical View of MgB_2 Core

The reacted powder and standard IMD wires were polished and their cross sections were observed under optical microscope. There is a clear distinction between MgB_2 layer and un-reacted Mg layer for the case of standard IMD sample, Figure 6.2.

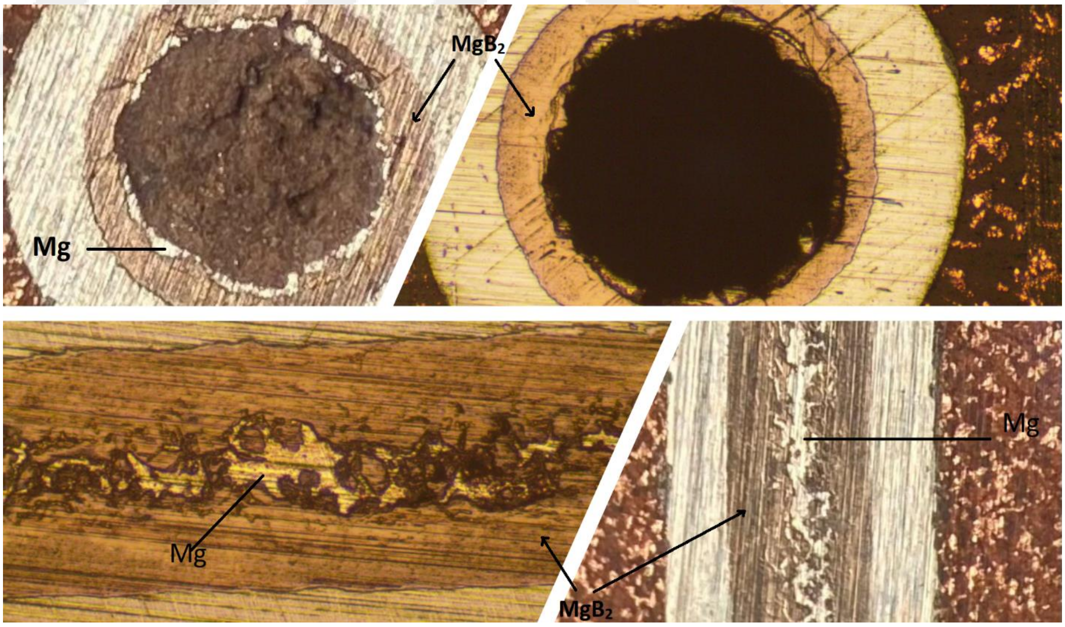

Figure 6.2. Cross section and longitudinal section views of core for Standard IMD heat treated wire. There is un-reacted layer of Mg for the case of Standard IMD wire.

The kinetics of MgB_2 phase formation in standard IMD wire can be divided into two stages. During Stage-I, heat treatment of the IMD wire results in a core that is depleted of Mg, surrounded by a thin cylinder of almost fully dense MgB_2, which was produced by the initial rapid infiltration of liquid Mg. In Stage-II, the reaction of the remaining B outside of this cylinder requires the diffusion of Mg through the dense MgB_2 inner layer. This causes drastic drop in Mg transport rate from infiltration to diffusion, stage-II proceeds slowly and leads to incomplete MgB_2 layer formation (75). By controlling the particle size of B or adjusting the rate of Mg diffusion into B, it is possible to prolong the duration, Stage-I, for the formation of a dense MgB_2 layer. As a result, the thickness of the MgB_2 layer can be expanded. So, it is obvious that remaining un-reacted Mg layer has caused the inferior superconducting behaviour in Standard IMD wire.

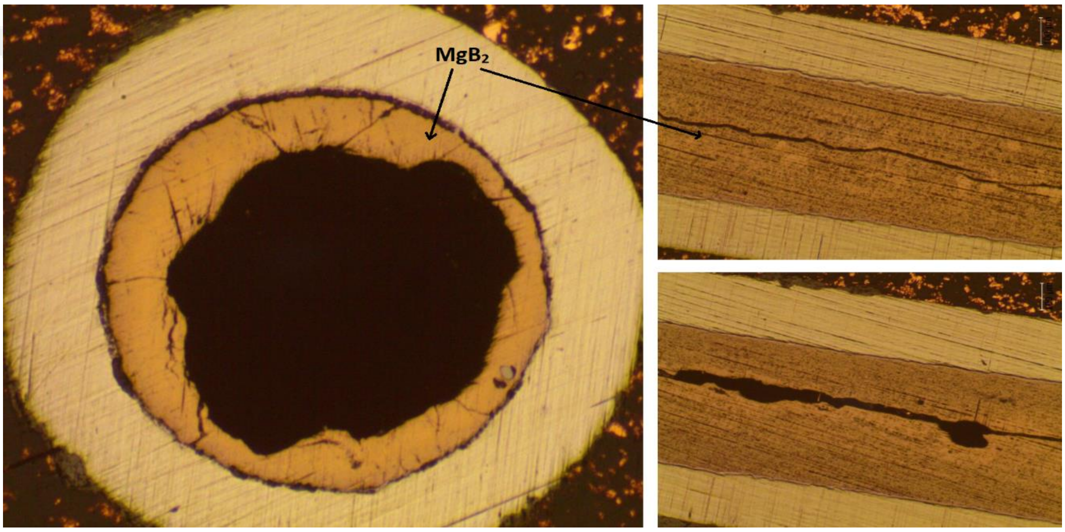

Figure 6.3. Cross section and longitudinal section views of core for powder IMD heat treated wire.

In Figure 6.3, powder IMD wire, there is no un-reacted layer of Mg and also there were no remnants of un-reacted Mg in the powder IMD wires identical as the one used in this work reported by Yetiş et al (52). The reaction and evaporation of Mg are directly proportional to its morphology (76). During the drawing process of powder IMD wire, the elongation of Mg particles causes an increase in the aspect ratio of Mg particles, as the wire is drawn to smaller and smaller diameters (66). The initial spherical Mg particles become elongated after wire drawing, resulting in a substantial increase in the free outer area per unit volume. The elongation of the initial composite Mg in powder method impacts the morphology of the Mg particles and increases the diffusion rate of Mg vapour into boron particles and results in the formation of fully dense MgB_2 layer (52).

6.2 The E-J Curves

The current-voltage measurements were carried out under an external magnetic field ranging between 0 to 5T at a temperature of 25K by using a closed-cycle cryostat system. In order to prevent Joule heating on the wire samples, the transport current running through the samples was linearly increased up to 1A maximum value. The critical current J_c values of the wires were calculated by using 1µV/cm criteria. The four probe method was used to measure voltage difference and a perpendicular magnetic field ($B \perp I$) was applied during measurements. The E-J curves were plotted by dividing the applied current to cross sectional area of MgB_2 layer, which was 1.87×10^{-3} cm^2 in powder IMD wire and 1.52×10^{-3} cm^2 in standard IMD wire.

Curves in Figures 6.4 and 6.5 show that the critical current density of powder IMD wire samples is 300 A-cm^{-2} while standard IMD wire samples can carry maximum current density 70 A-cm^{-2} before transition to normal state in the applied field of 5T at 25K. That means the powder IMD wires have the capability to carry four times larger critical current than the standard IMD wires.

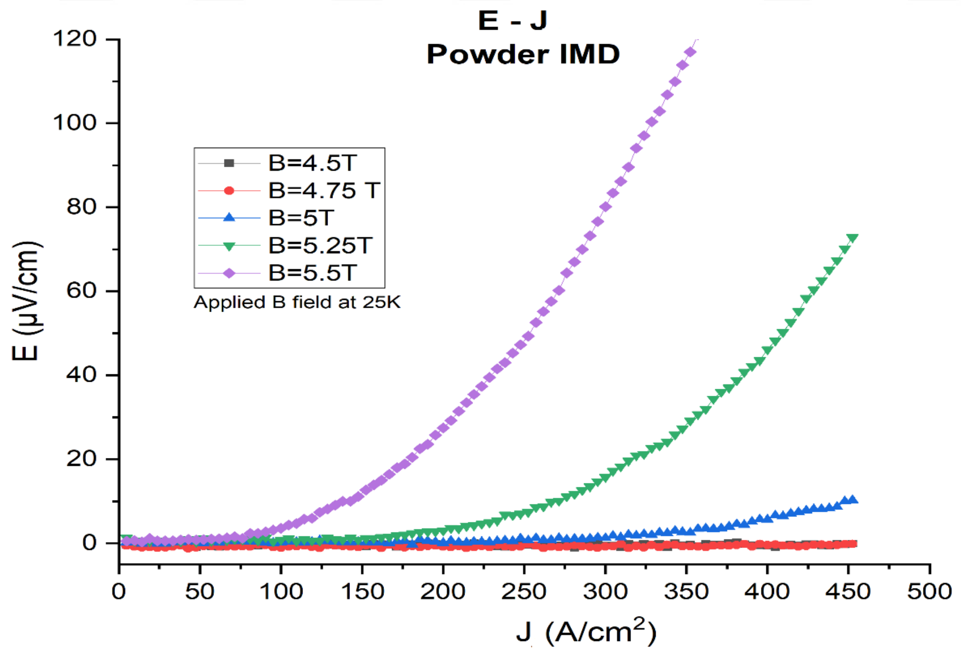

Figure 6.4. E-J curves for Powder IMD wire, at 25K in different B fields. 4.5T and 4.75T curves lie on top of each other.

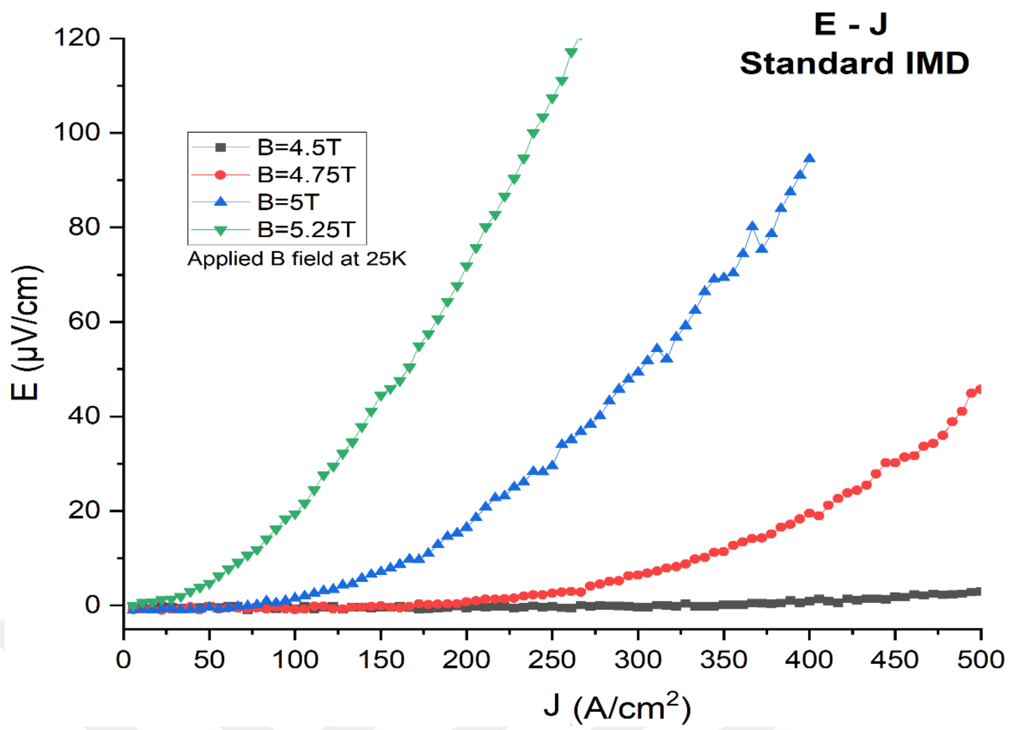

Figure 6.5. E-J curves for Powder IMD wire, at 25K in different B fields.

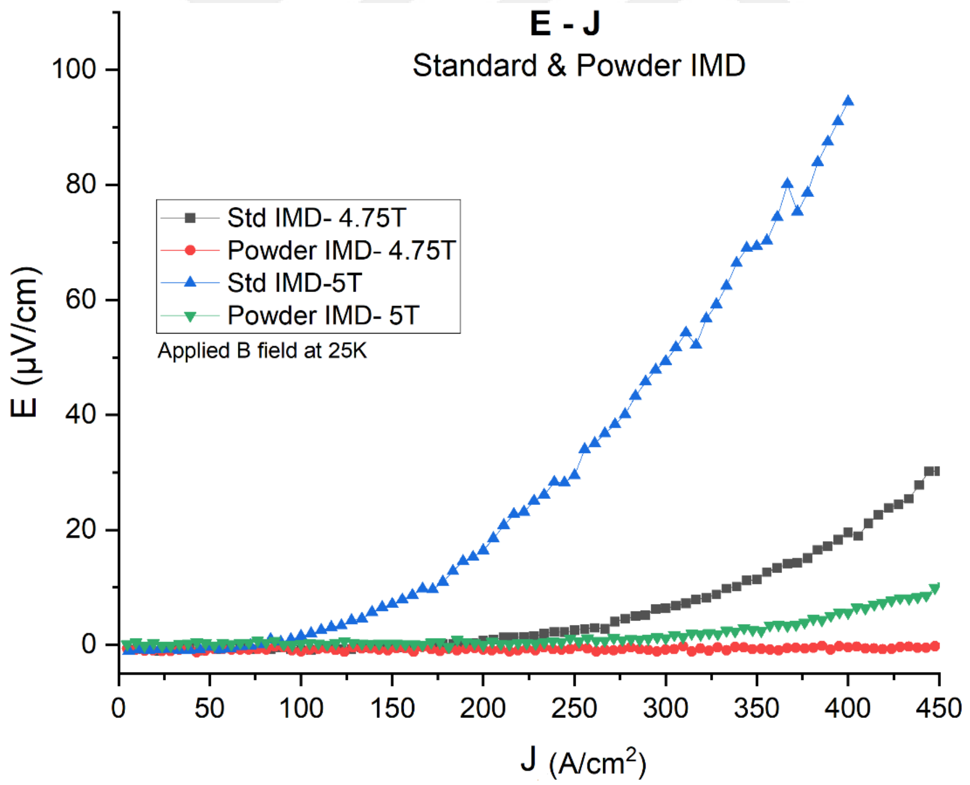

Figure 6.6. Comparison of E-J curves for Powder and Standard IMD wires, at 25K in different B fields.

By observing E-J curves in Figure 6.6, it is obvious that powder IMD wires show better current voltage behaviour than standard IMD wires do. By observing the above graph, standard IMD wire shows transition to normal state at lower current density under 4.75T magnetic field. However, under a magnetic field of 5T, powder IMD wire is superconducting without any transition to normal state. Being more specific, in the applied magnetic field of 4.75T at 25K, powder IMD wire can carry a current density above 450 $A\text{-}cm^{-2}$ while standard IMD wire can carry 200 $A\text{-}cm^{-2}$, which is nearly half for powder IMD wire. Also, it has been estimated by Yetiş et al (77) that powder IMD wires present potential for even higher I_c values at 25K in external magnetic fields.

6.3 Evaluation of Cross Sectional Areas of Samples

The cross sectional areas of iron, boron and magnesium regions were measured using the Kameram software on an optical microscope with a 5× magnification, to observe deformation effect on different regions during cold drawing. By observing Figure 6.7, the cross sectional areas of iron regions of different diameters for both powder and standard IMD wires are nearly same. Also for the case of boron and magnesium regions, the cross sectional areas are quite similar for both wires as shown in Figures 6.8 and 6.9. This behaviour shows a good homogeneity of boron and magnesium during cold wire drawing, which improves the superconducting properties of the wires.

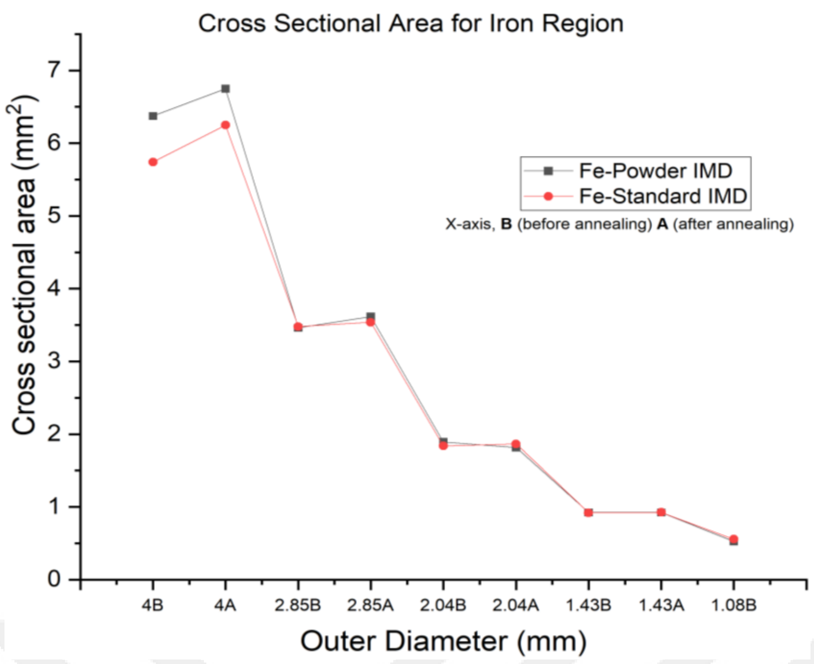

Figure 6.7. Cross sectional area of iron regions for powder and standard IMD wires having different diameters.

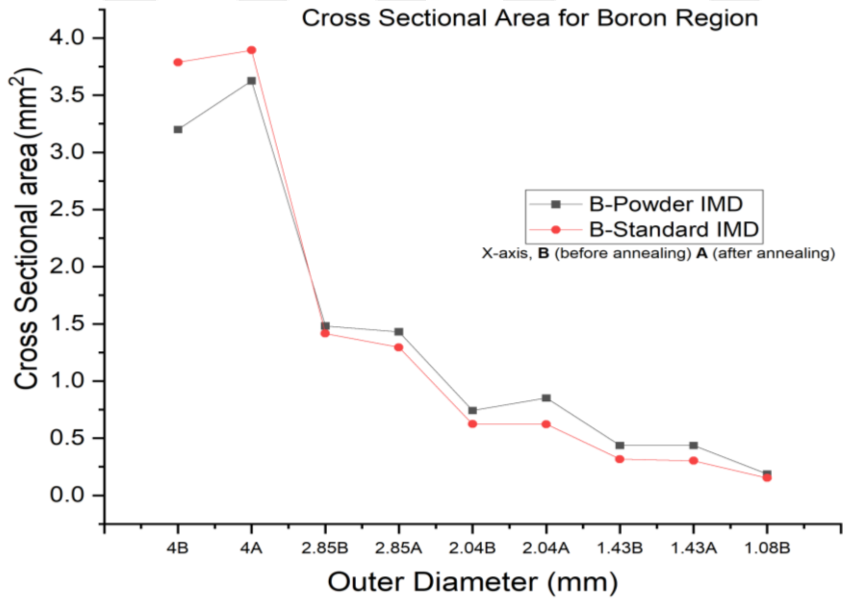

Figure 6.8. Cross sectional area of boron regions for powder and standard IMD wires having different diameters.

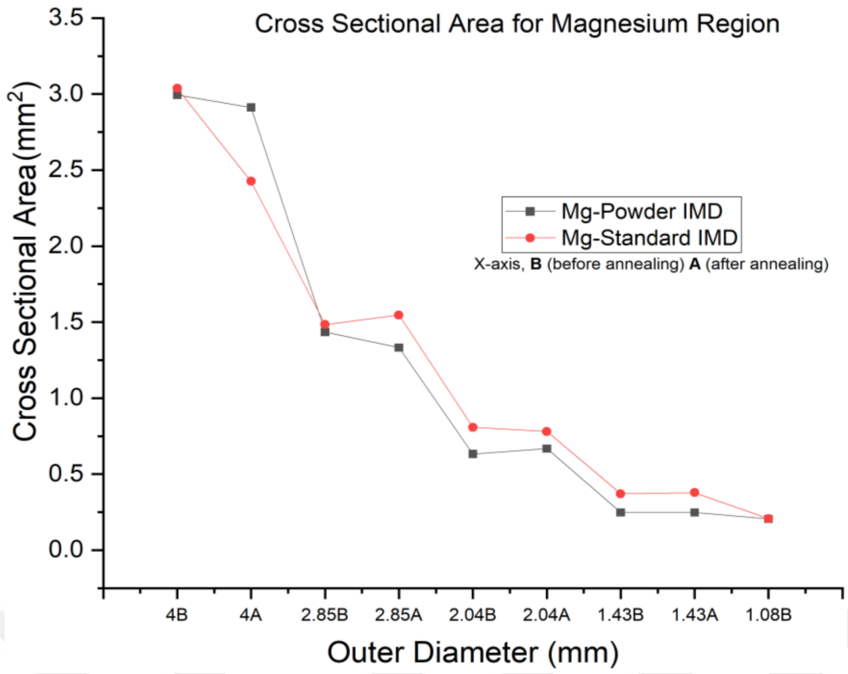

Figure 6.9. Cross sectional area of magnesium regions for powder and standard IMD wires having different diameters.

Cold drawing was performed for both standard IMD and powder IMD wires until the outer diameter was reduced to 1.08mm. During cold drawing, cross sectional areas of samples having different diameters were measured for both wires, and cross sectional areas were quite similar for both wires. That indicates homogeneity of boron and magnesium inside iron sheath and nearly same amount of compression during deformation. Initially (before cold drawing) the diameter of magnesium region was 6mm in powder IMD wire and the diameter of magnesium region in standard IMD wire was 4.66mm. Even though the diameter of Mg region in powder IMD wire was larger than that of standart IMD wire, both wires had the same diameter of magnesium region after cold drawing (deformation). This indicates that more stress has been accumulated during the cold drawing on powder IMD wire than standard IMD wire.

6.4 Vickers Hardness Test

Hardness of magnesium, boron and iron layers in powder and standard IMD wire were measured. There were total 18 samples, 9 samples for powder IMD wire and 9 samples for standard IMD wire having different diameters. Hardness was measured after every 30% reduction of diameter during cold drawing and also after applying intermediate heat treatment, to observe the behaviour of heat treatment for different regions.

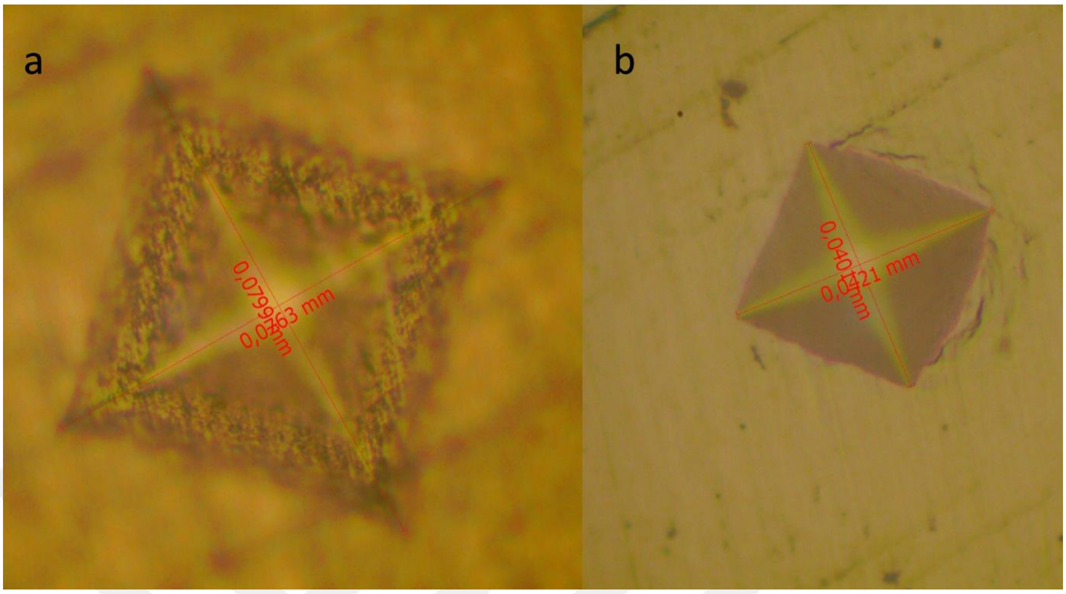

Figure 6.10. The indentation traces of (a) Mg region and (b) iron region.

Figure 6.10 shows the indentation traces on magnesium and iron regions. 1.96N force was applied on iron Fe regions in the powder and standard wires to measure HV, the hardness was nearly same before and after strain relief heat treatment for different diameters. As shown in Figure 6.11, there was linear increment in hardness as there was reduction in diameter during cold drawing of both wires. For final outer diameter of 1.08mm, hardness of iron regions were same for both wires.

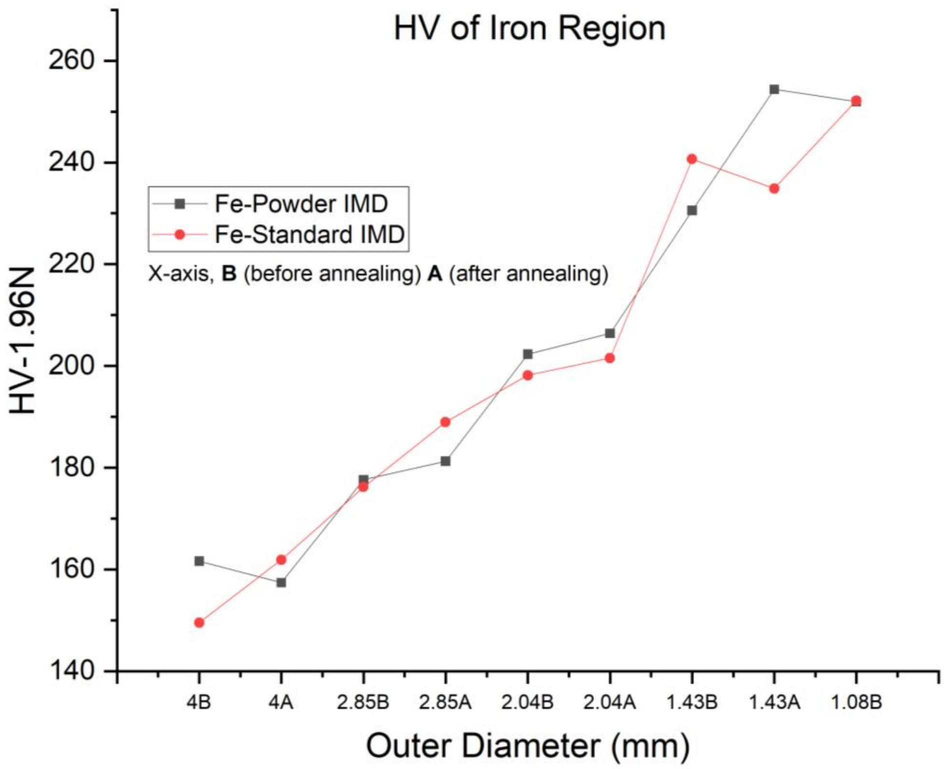

Figure 6.11. HV of iron region for powder and standard IMD wire samples having different outer diameters.

For the case of boron regions, the 0.098N force was used to measure HV. First and final values of HV for boron regions in powder and standard IMD samples were same, while there was deviation in middle values as shown in Figure 6.12. Usually the indentation traces of boron regions are not quite clear, this may hinder the precise measurement of traces and it might have caused larger error margins. Boron regions in the wire diameters of 2.85mm and 2.04mm showed larger HV value for powder IMD wire than standard IMD wire. Whereas initial diameter 4mm and final diameter 1.08mm showed the same HV of boron regions for standard and powder IMD samples. There was sudden increment of HV values of boron regions in powder IMD wire for the samples having outer diameter 2.85 mm and 2.04 mm, it could be due to instabilities resulting from powder structure of the boron layer.

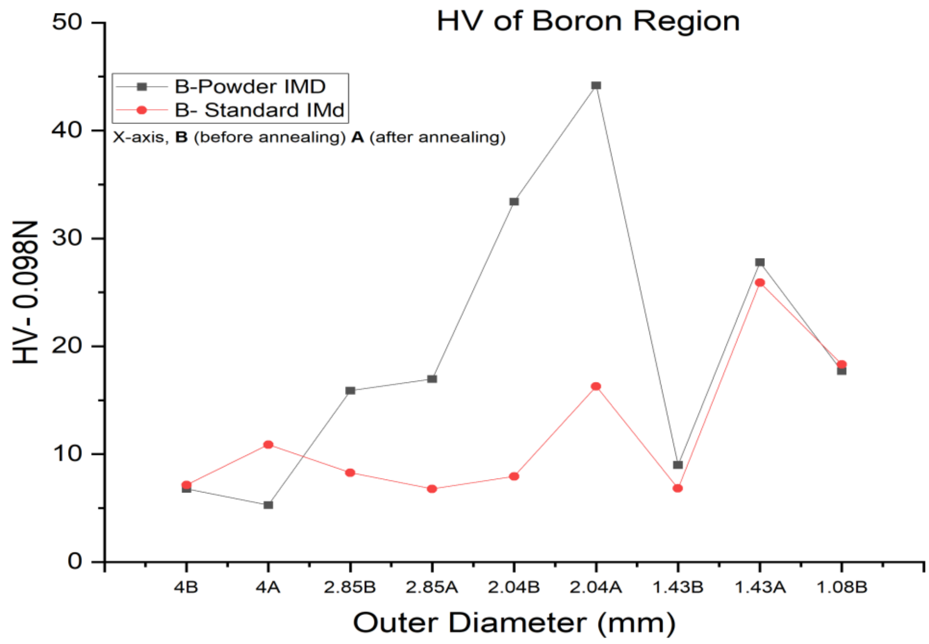

Figure 6.12. HV of boron regions for powder and standard IMD wire samples having different outer diameters.

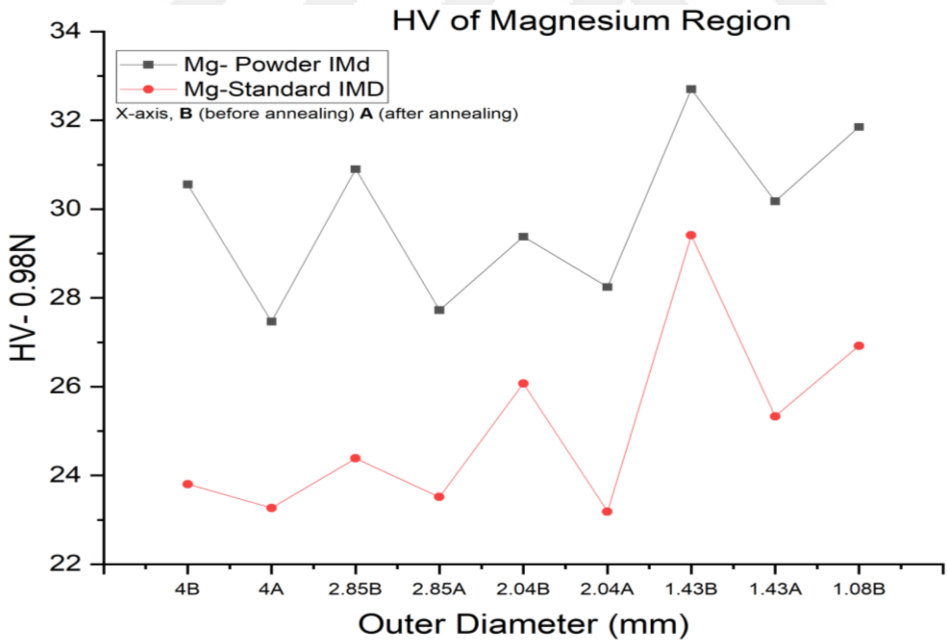

Figure 6.13. HV of magnesium regions for powder and standard IMD wire samples having different outer diameters.

In the case of Mg regions, the 0.98N force was applied. It is clearly obvious from Figure 6.13 that Mg regions of powder IMD wire showing higher HV values than standard IMD wire samples. Microhardness of magnesium regions in all samples decreases after intermediate annealing for both powder and standard IMD wires. It is crucial to note that when exposed to air, magnesium readily forms oxides, resulting in the formation of MgO and $Mg(OH)_2$ layers (78) . Furthermore, the thermal expansion coefficient of magnesium hydroxide is greater than that of magnesium, leading to compressive stress within the magnesium hydroxide layer. Subsequently, upon annealing at temperatures above 200°C, $Mg(OH)_2$ decomposes into MgO, creating nano-sized pores within the oxide layers (79). These pores can be filled during the cold drawing process, thereby enhancing the microhardness of magnesium in powder IMD wire. In addition, it has been reported that presence of MgO in magnesium powder increases the microhardness of Mg (containing MgO) during powder metallurgy (80).

Furthermore, HV results showed that the microhardness of iron and boron regions in powder and standard IMD wires with different diameters were nearly same. Mg rod was used in standard IMD and Mg powder was used in powder IMD wires. However, magnesium regions in powder IMD wire samples showed higher microhardness than magnesium regions in standard IMD wire samples. This can also be contributed to the work softening behaviour of Mg rod during cold drawing.

As magnesium is highly reactive with oxygen, so there is high possibility of MgO formation during filling and powder IMD wire formation process. The MgO particles form good interfacial bonding with Mg particles and cause to decrease porosity during cold drawing. So, enhancement of microhardness of Mg region in powder IMD wire during cold drawing is promising from mechanical perspective for the production of long wires since a small increase in MgO content can be justified when cross sectional uniformity along the wire is improved.

7. CONCLUSION

In this study, two different types of wires were fabricated using powder and standard IMD methods. The powder IMD wires show better superconducting behaviour than standard IMD wires. The HV results indicated that the microhardness of iron region was nearly same in both standard and powder IMD wire but microhardness of the magnesium region was enhanced during the cold drawing process for powder IMD wire compared to the standard IMD wire. Hence, mechanical behaviour of powder IMD wire makes the drawing process safe since mechanical strength improves drawing process.

There was a difference of 0.5K between the superconducting transition temperatures of standard and powder IMD wires, superconducting properties of standard IMD wire was suppressed by un-reacted Mg layer when both wires were sintered at 650^{o}C for 1h. J-E behaviour of powder IMD wire at 5T is better than that of standart IMD wire at 4.75T. So, powder IMD wires are more promising than standard IMD wires in terms of superconducting properties.

8. REFERENCES

Vancouver citation system was used in this thesis.

1. Buckel W, Kleiner R. Superconductivity: fundamentals and applications. John Wiley & Sons; 2008.

2. Van Delft D, Kes P. The discovery of superconductivity. Phys Today. 2010;63(9):38–43.

3. Forrest AM. Meissner and Ochsenfeld revisited. Eur J Phys. 1983;4(2):117.

4. Reynolds CA, Serin B, Wright WH, Nesbitt LB. Superconductivity of isotopes of mercury. Phys Rev. 1950;78(4):487.

5. Maxwell E. Isotope effect in the superconductivity of mercury. Phys Rev. 1950;78(4):477.

6. London F, London H. The electromagnetic equations of the supraconductor. Proc R Soc Lond Ser -Math Phys Sci. 1935;149(866):71–88.

7. Pippard AB, Bragg WL. An experimental and theoretical study of the relation between magnetic field and current in a superconductor. Proc R Soc Lond Ser Math Phys Sci. 1953;216(1127):547–68.

8. Bardeen J. Theory of the Meissner effect in superconductors. Phys Rev. 1955;97(6):1724.

9. Barua S. Economical production of high performance MgB2 superconductor with improved grain connectivity. 2015;

10. Cooper LN. Bound electron pairs in a degenerate Fermi gas. Phys Rev. 1956;104(4):1189.

11. Bardeen J, Cooper LN, Schrieffer JR. Theory of superconductivity. Phys Rev. 1957;108(5):1175.

12. Zhou T. Mechanism of high temperature superconductivity-the BCS theory and a new electron pairing medium.

13. Josephson BD. Possible new effects in superconductive tunnelling. Phys Lett. 1962;1(7):251–3.

14. Bednorz JG, Müller KA. Possible high T c superconductivity in the Ba- La- Cu- O system. Z Für Phys B Condens Matter. 1986;64(2):189–93.

15. Wu MK, Ashburn JR, Torng C, Hor PH, Meng RL, Gao L, et al. Superconductivity at 93 K in a new mixed-phase Y-Ba-Cu-O compound system at ambient pressure. Phys Rev Lett. 1987;58(9):908.

16. Schilling A, Cantoni M, Guo JD, Ott HR. Superconductivity above 130 k in the hg–ba–ca–cu–o system. Nature. 1993;363(6424):56–8.

17. Nagamatsu J, Nakagawa N, Muranaka T, Zenitani Y, Akimitsu J. Superconductivity at 39 K in magnesium diboride. nature. 2001;410(6824):63–4.

18. Vinod K, Kumar RA, Syamaprasad U. Prospects for MgB2 superconductors for magnet application. Supercond Sci Technol. 2006;20(1):R1.

19. Linares RN. Hundred years of Superconducting Materials. 2010;

20. Nishibori E, Takata M, Sakata M, Tanaka H, Muranaka T, Akimitsu J. Bonding nature in MgB2. J Phys Soc Jpn. 2001;70(8):2252–4.

21. Rettaroli A, Salamanna G, Gatti DC. Characterization of superconducting resonant RF cavities for axion search with the QUAX experiment. Master Degree Thesis Phys Dept Univ Roma 3. 2018;

22. LLOSA PC. Preparation of GdBa2Cu3O7 superconducting films by chemical solution deposition.

23. Seidel P. Applied superconductivity: handbook on devices and applications. John Wiley & Sons; 2015.

24. Ravindran P, Vajeeston P, Vidya R, Kjekshus A, Fjellvåg H. Detailed electronic structure studies on superconducting MgB 2 and related compounds. Phys Rev B. 2001;64(22):224509.

25. Choi HJ, Roundy D, Sun H, Cohen ML, Louie SG. The origin of the anomalous superconducting properties of MgB2. Nature. 2002;418(6899):758–60.

26. Buzea C, Yamashita T. Review of the superconducting properties of MgB2. Supercond Sci Technol. 2001;14(11):R115.

27. An JM, Pickett WE. Superconductivity of MgB 2: covalent bonds driven metallic. Phys Rev Lett. 2001;86(19):4366.

28. Mazin II, Antropov VP. Electronic structure, electron–phonon coupling, and multiband effects in MgB2. Phys C Supercond. 2003;385(1–2):49–65.

29. Kortus J, Mazin II, Belashchenko KD, Antropov VP, Boyer LL. Superconductivity of metallic boron in MgB 2. Phys Rev Lett. 2001;86(20):4656.

30. Golubov AA, Kortus J, Dolgov OV, Jepsen O, Kong Y, Andersen OK, et al. Specific heat of MgB2 in a one-and a two-band model from first-principles calculations. J Phys Condens Matter. 2002;14(6):1353.

31. Scalapino DJ. The case for dx2- y2 pairing in the cuprate superconductors. Phys Rep. 1995;250(6):329–65.

32. Kotegawa H, Ishida K, Kitaoka Y, Muranaka T, Nakagawa N, Takagiwa H, et al. Evidence for strong-coupling s-wave superconductivity in MgB2: 11B-NMR study of MgB2 and the related materials. Phys C Supercond. 2002;378:25–32.

33. Chen K, Dai W, Zhuang CG, Li Q, Carabello S, Lambert JG, et al. Momentum-dependent multiple gaps in magnesium diboride probed by electron tunnelling spectroscopy. Nat Commun. 2012;3(1):619.

34. Lyard L, Samuely P, Szabo P, Klein T, Marcenat C, Paulius L, et al. Anisotropy of the upper critical field and critical current in single crystal MgB 2. Phys Rev B. 2002;66(18):180502.

35. Mourachkine A. Room-temperature superconductivity. Cambridge Int Science Publishing; 2004.

36. Bud'ko SL, Lapertot G, Petrovic C, Cunningham CE, Anderson N, Canfield PC. Boron isotope effect in superconducting MgB 2. Phys Rev Lett. 2001;86(9):1877.

37. Hata S, Yoshidome T, Sosiati H, Tomokiyo Y, Kuwano N, Matsumoto A, et al. Microstructures of MgB2/Fe tapes fabricated by an in situ powder-in-tube method using MgH2 as a precursor powder. Supercond Sci Technol. 2006;19(2):161.

38. Martínez E, Mikheenko P, Martínez-López M, Millán A, Bevan A, Abell JS. Flux pinning force in bulk mg b 2 with variable grain size. Phys Rev B. 2007;75(13):134515.

39. Matsushita T, Kiuchi M, Yamamoto A, Shimoyama J, Kishio K. Critical current density and flux pinning in superconducting MgB2. Phys C Supercond. 2008;468(15–20):1833–5.

40. Collings EW, Sumption MD, Bhatia M, Susner MA, Bohnenstiehl SD. Prospects for improving the intrinsic and extrinsic properties of magnesium diboride superconducting strands. Supercond Sci Technol. 2008;21(10):103001.

41. Yan G, Feng Y, Fu BQ, Liu CF, Zhang PX, Wu XZ, et al. Effect of synthesis temperature on density and microstructure of MgB 2 superconductor at ambient pressure. J Mater Sci. 2004;39:4893–8.

42. Authors C, III/17E-17F-41C editors of the volumes. Boron (B) density, heat capacity, amorphous boron. Non-Tetrahedrally Bond Elem Bin Compd I. 1998;1–4.

43. Li GZ, Sumption MD, Susner MA, Yang Y, Reddy KM, Rindfleisch MA, et al. The critical current density of advanced internal-Mg-diffusion-processed MgB2 wires. Supercond Sci Technol. 2012;25(11):115023.

44. Yan SC, Yan G, Liu CF, Lu YF, Zhou L. Experimental study on the phase formation for the Mg–B system in Ar atmosphere. J Alloys Compd. 2007;437(1–2):298–301.

45. Glowacki BA, Majoros M, Vickers M, Evetts JE, Shi Y, McDougall I. Superconductivity of powder-in-tube MgB2 wires. Supercond Sci Technol. 2001;14(4):193.

46. Kutukcu MN, Atamert S, Scandella JL, Hopstock R, Blackwood AC, Dhulst C, et al. Composite superconducting MgB 2 wires made by continuous process. IEEE Trans Appl Supercond. 2018;28(4):1–4.

47. Giunchi G, Ceresara S, Ripamonti G, Di Zenobio A, Rossi S, Chiarelli S, et al. High performance new MgB2 superconducting hollow wires. Supercond Sci Technol. 2003;16(2):285.

48. 葉術軍. Development of high performance MgB2 superconducting wires [PhD Thesis]. 九州大学; 2014.

49. Sun Y, Zhang P, Wang Q, Qi M, Yang F, Jiao G, et al. Investigation of Nb–B Diffusion and the Superconducting Properties of MgB 2/Nb/Cu Tapes. J Supercond Nov Magn. 2012;25:943–50.

50. Hur JM, Togano K, Matsumoto A, Kumakura H, Wada H, Kimura K. Fabrication of high-performance MgB2 wires by an internal Mg diffusion process. Supercond Sci Technol. 2008;21(3):032001.

51. Wang D, Ma Y, Yao C, Xu D, Zhang X, Awaji S. Transport properties of multifilament MgB2 long wires and coils prepared by an internal Mg diffusion process. Supercond Sci Technol. 2017;30(6):064003.

52. Yetiş H, Avcı D, Karaboğa F, Gajda D, Akdoğan M, Belenli İ. An innovative approach to fabricate MgB2/Fe IMD wires by magnesium powder method. Phys B Condens Matter. 2020;593:412277.

53. Gajda D, Morawski A, Zaleski AJ, Cetner T, Häßler W, Nenkov K, et al. Significant enhancement of the critical current of MgB2 wires through a reduction of the diameter using HIP method. Scr Mater. 2018;143:77–80.

54. Hossain MSA, Motaman A, Barua S, Patel D, Mustapic M, Kim JH, et al. The roles of CHPD: superior critical current density and n-value obtained in binary in situ MgB2 cables. Supercond Sci Technol. 2014;27(9):095016.

55. Mikheenko P. Superconductivity for hydrogen economy. In: Journal of Physics: Conference Series. IOP Publishing; 2011. p. 012014.

56. Yamada H, Hirakawa M, Kumakura H, Kitaguchi H. Effect of aromatic hydrocarbon addition on in situ powder-in-tube processed MgB2 tapes. Supercond Sci Technol. 2006;19(2):175.

57. Berenov A, Serquis A, Liao XZ, Zhu YT, Peterson DE, Bugoslavsky Y, et al. Enhancement of critical current density in low level Al-doped MgB2. Supercond Sci Technol. 2004;17(10):1093.

58. Rafieazad M, BALCI Ö, Selçuk A, Somer M. Review on magnesium diboride (MgB2) as excellent superconductor: Effects of the production techniques on the superconducting properties. J Boron. 2017;2(2):87–96.

59. Wang J, Bugoslavsky Y, Berenov A, Cowey L, Caplin AD, Cohen LF, et al. High critical current density and improved irreversibility field in bulk MgB 2 made by a scaleable, nanoparticle addition route. Appl Phys Lett. 2002;81(11):2026–8.

60. Rui XF, Zhao Y, Xu YY, Zhang L, Sun XF, Wang YZ, et al. Improved flux pinning behaviour in bulk MgB2 achieved by nano-SiO2 addition. Supercond Sci Technol. 2004;17(4):689.

61. Ueda S, Shimoyama J ichi, Yamamoto A, Horii S, Kishio K. Enhanced critical current properties observed in Na2CO3-doped MgB2. Supercond Sci Technol. 2004;17(7):926.

62. Ulgen AT, Belenli I. The Effect of Fe Diffusion on Some Physical and Superconducting Properties of MgB 2. J Supercond Nov Magn. 2017;30:1089–95.

63. Lin Q, Chen S, Shen B, Sun F. CVD diamond coated drawing dies: a review. Mater Manuf Process. 2021;36(4):381–408.

64. Dodyim N, Yoshida K, Murata T, Kobayashi Y. Drawing of magnesium fine wire and medical application of drawn wire. Procedia Manuf. 2020;50:271–5.

65. Sun L, Bai J, Xue F, Chu C, Meng J. The work softening behavior of pure Mg wire during cold drawing. Materials. 2018;11(4):602.

66. Susner MA, Daniels TW, Sumption MD, Rindfleisch MA, Thong CJ, Collings EW. Drawing induced texture and the evolution of superconductive properties with heat treatment time in powder-in-tube in situ processed MgB2 strands. Supercond Sci Technol. 2012;25(6):065002.

67. Hossain MSA, Senatore C, Flükiger R, Rindfleisch MA, Tomsic MJ, Kim JH, et al. The enhanced Jc and Birr of in situ MgB2 wires and tapes alloyed with C4H6O5 (malic acid) after cold high pressure densification. Supercond Sci Technol. 2009;22(9):095004.

68. Li GZ, Sumption MD, Zwayer JB, Susner MA, Rindfleisch MA, Thong CJ, et al. Effects of carbon concentration and filament number on advanced internal Mg infiltration-processed MgB2 strands. Supercond Sci Technol. 2013;26(9):095007.

69. Park DK, Ling J, Rindfleisch M, Voccio J, Hahn S, Bascuñán J, et al. $${$$\backslash$rm MgB$}$ _ ${$2$}$ $ for MRI Magnets: Test Coils and Superconducting Joints Results. IEEE Trans Appl Supercond. 2012;22(3):4400305–4400305.

70. Nam GD, Sung HJ, Go BS, Park M, Yu IK. Design and comparative analysis of MgB2 and YBCO wire-based-superconducting wind power generators. IEEE Trans Appl Supercond. 2018;28(3):1–5.

71. Ye L, Majoros M, Campbell AM, Coombs T, Astill D, Harrison S, et al. Experimental studies of the quench behaviour of MgB2 superconducting wires for fault current limiter applications. Supercond Sci Technol. 2007;20(7):621.

72. Zhang D, Sumption MD, Majoros M, Kovacs C, Collings EW, Panik D, et al. Quench, normal zone propagation velocity, and the development of an active protection scheme for a conduction cooled, react-and-wind, MgB2 MRI coil segment. Supercond Sci Technol. 2019;32(12):125003.

73. Meng J, Sun L, Zhang Y, Xue F, Chu C, Bai J. Evolution of recrystallized grain and texture of cold-drawn pure Mg wire and their effect on mechanical properties. Materials. 2020;13(2):427.

74. Al-Joubori AA, Suryanarayana C. Synthesis and thermal stability of homogeneous nanostructured Fe 3 C (cementite). J Mater Sci. 2018;53:7877–90.

75. Li GZ, Sumption MD, Collings EW. Kinetic analysis of MgB2 layer formation in advanced internal magnesium infiltration (AIMI) processed MgB2 wires. Acta Mater. 2015;96:66–71.

76. Cheng F, Ma Z, Yu L, Li C, Liu C, Guo Q, et al. Effects of morphology of Mg powder precursor on phase formation and superconducting properties of Mg 11 B 2 low activation superconductor. J Mater Chem C. 2018;6(30):8069–75.

77. Yetiş H, Avcı D, Karaboğa F, Aksoy C, Gajda D, Martínez E, et al. Transport and structural properties of MgB2/Fe wires produced by redesigning internal Mg diffusion process. Supercond Sci Technol. 2022;35(4):045012.

78. Jeon KJ, Moon HR, Ruminski AM, Jiang B, Kisielowski C, Bardhan R, et al. Air-stable magnesium nanocomposites provide rapid and high-capacity hydrogen storage without using heavy-metal catalysts. Nat Mater. 2011;10(4):286–90.

79. Karimpour M, Eatezadi SR, Hasani S, Ghaei A. The oxidation mechanism of pure magnesium powder particles: a mathematical approach. Metall Mater Trans B. 2019;50:1597–607.

80. Goh CS, Gupta M, Wei J, Lee LC. Characterization of high performance Mg/MgO nanocomposites. J Compos Mater. 2007;41(19):2325–35.